Genetic-tracing of CD8+ T cell fate decisions

Kok, L.

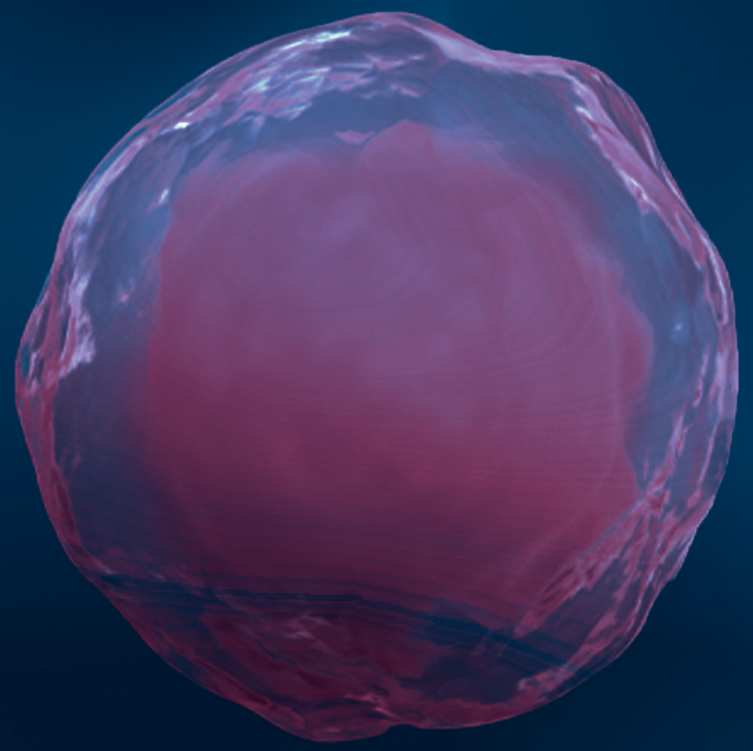

3.2

Replicative history marks transcriptional and functional disparity in the CD8$^+$ T cell memory pool

Kaspar Bresser[1,*], Lianne Kok[1,*], Arpit C. Swain[2], Lisa A. King[1,3], Laura Jacobs[1], Tom S. Weber[4], Leila Perié[5], Ken R. Duffy[6], Rob J. de Boer[2], Ferenc A. Scheeren[7#] and Ton N. Schumacher[1,8#]

Nat Immunol. 2022 May;23(5):791-801.
doi: 10.1038/s41590-022-01171-9

1 Division of Molecular Oncology & Immunology, Oncode Institute, The Netherlands Cancer Institute, Amsterdam, The Netherlands
2 Theoretical Biology and Bioinformatics, Utrecht University, Utrecht, The Netherlands.
3 Present address: Department of Medical Oncology, Amsterdam UMC, Vrije Universiteit Amsterdam, Cancer Center Amsterdam, Amsterdam, The Netherlands.
4 The Walter and Eliza Hall Institute of Medical Research, Parkville, Victoria, Australia.
5 Institut Curie, PSL Research University, CNRS UMR168, Paris, France.
6 Hamilton Institute, Maynooth University, Maynooth, Ireland.
7 Department of Medical Oncology, Leiden University Medical Center, Leiden, Netherlands
8 Division of Immunohematology and Blood transfusion, Leiden University Medical Center, Leiden, The Netherlands
* These authors contributed equally to this work
# To whom correspondence should be addressed at f.a.scheeren@lumc.nl; t.schumacher@nki.nl

Keywords
Proliferation dynamics; lineage tracing; Probabilistic labeling, Replicative history; T cell memory;

ABSTRACT

Clonal expansion is a core aspect of T cell immunity. However, little is known with respect to the relationship between replicative history and the formation of distinct CD8$^+$ memory T cell subgroups. To address this issue, we developed a genetic-tracing approach, termed the DivisionRecorder, that reports the extent of past proliferation of cell pools *in vivo*. Using this system to genetically 'record' the replicative history of different CD8$^+$ T cell populations throughout a pathogen-specific immune response, we demonstrate that the central memory T cell (T_{CM}) pool is marked by a higher number of prior divisions than the effector memory T cell pool, due to the combination of strong proliferative activity during the acute immune response and selective proliferative activity after pathogen clearance. Furthermore, by combining DivisionRecorder analysis with single cell transcriptomics and functional experiments, we show that replicative history identifies distinct cell pools within the T_{CM} compartment. Specifically, we demonstrate that lowly divided T_{CM} display enriched expression of stem-cell-associated genes, exist in a relatively quiescent state, and are superior in eliciting a proliferative recall response upon activation. These data provide the first evidence that a stem cell like memory T cell pool that reconstitutes the CD8$^+$ T cell effector pool upon reinfection is marked by prior quiescence.

INTRODUCTION

The CD8$^+$ T cell compartment serves to provide protection against intracellular pathogens and also acts as a modifier of cancer growth. Upon antigen encounter, naïve T cells (T_N) undergo extensive gene-expression alterations, while entering a highly proliferative state, dividing every 4h to 6h[1,2] in mice. This phase of clonal expansion gives rise to a phenotypically and functionally diverse pool of effector T cells (T_{EFF}) that exceeds its precursor population size by >10,000-fold[3,4]. Unlike T_N, these T_{EFF} have the capacity to disseminate to peripheral tissues, and scan for and kill infected or transformed cells. Upon antigen clearance, around 95% of the T_{EFF} pool succumbs to apoptosis, leaving behind a small long-lived pool of memory T cells (T_M) that is equipped to provide long-term protection against recurring pathogens.

The central role of proliferation in the T cell response has inspired many to study the relationship between replication and T cell state. While earlier work hinted that memory precursor T cells have undergone limited clonal expansion[5,6], more recent work studying acute T cell responses in human subjects demonstrated that T_M, as a whole, are derived from precursor cells that have undergone an extensive number of divisions[7]. Furthermore, prior work has shown that cell cycle speed can differ substantially between phenotypically distinct T cell subsets at different time-points in the T cell response. Specifically, central memory T cells (T_{CM}), a subgroup of memory cells that are endowed with a high level of multipotency, have been documented to undergo homeostatic proliferation after pathogen clearance, while effector memory T cells (T_{EM}) have a low turnover rate[8,9]. In contrast, during the effector phase, a T_{CM}-like state has been linked to lower division speed and reduced clonal burst size compared to their T_{EM}-like and terminally differentiated counterparts[10–13].

The phase-dependent association of proliferative activity within specific cell states, in combination with the reported phenotypic instability of certain T cell subsets[14,15], makes it difficult to deduce the replicative history (i.e., the cumulative number of prior divisions) of different memory T cell populations, and the possible relationship between such replicative history and functional properties. Here, we develop a genetic-tracing approach—termed DivisionRecorder—that allows the measurement of prior division of cell pools over extensive rounds of division, and apply this approach to determine to what extent replicative history identifies distinct memory T cell states and behaviors. In this effort, we focus on three central issues: (1) What are the differences in replicative history between (precursor-)T_{CM} and T_{EM} in the effector and memory phase? (2) Is there heterogeneity in prior division within the T_{CM} pool? (3) If so, does replicative history of cells within the T_{CM} pool predict their capacity to mount a secondary T cell response?

RESULTS

Division-linked genetic labeling of cell pools.

The genome contains a large number of hypervariable short tandem nucleotide repeats (STRs) that accumulate intra-allelic length mutations through DNA polymerase slippage during cell division. Such slippage mutations in endogenous STRs have been used to study lineage trees in various organisms and tissues[16,17], and synthetic STRs have previously been employed in a probabilistic labeling approach to define stem cells in the intestinal epithelium and the mammary gland[18,19]. To investigate the replicative history of memory T cells, we engineered a synthetic STR-reporter system to continuously 'record' proliferation in cell pools. This genetically encoded system, termed DivisionRecorder, utilizes a synthetic STR domain to achieve a division-linked low-probability acquisition of a fluorescent mark (**Fig. 1a**). The DivisionRecorder consists of two separate elements: (1) a retroviral-vector encoded module that contains a synthetic STR linked to an out-of-frame CRE recombinase gene; (2) A CRE-activity reporter module that irreversibly induces the expression of a red fluorescent protein (RFP). In its base configuration, all cells that contain the DivisionRecorder only express GFP (hereafter referred to as DR^{GFP} cells). As cells undergo successive divisions, slippage mutations that occur within the synthetic STR yield in-frame variants of the downstream CRE recombinase gene at a fixed, division-dependent, probability (p). The resulting CRE activity induces an irreversible activation of the RFP gene, giving rise to GFP^+RFP^+ cells (hereafter referred to as DR^{RFP}) that pass this genetically encoded label on to subsequent generations, resulting in a cumulative increase in the DR^{RFP} cell fraction within the $DivisionRecorder^+$ (DR^+, i.e., the sum of DR^{GFP} and DR^{RFP}) population as the cell pool expands (**Fig. 1b, Supplementary Note 1**). Importantly, when p is small (< 0.01) the DivisionRecorder yields a near-linear relationship between the DR^{RFP} fraction and the average number of divisions over dozens of population doublings (**Fig. 1c**)[20], thereby allowing analysis of replicative history—at the population level—far beyond what can be achieved with classical cell labeling dyes[21] (**Fig. 1d**).

To test the utility of the DivisionRecorder, we established a reporter cell-line carrying a lox-STOP-lox-RFP cassette. Following retroviral introduction of the GFP-STR-CRE module, a progressive increase in DR^{RFP} cells was observed over time, whereas no label acquisition was observed when the STR was replaced with a stable DNA sequence (**Fig 1e, f**). Moreover, the rate at which DR^{RFP} cells accumulated was dependent on the sequence stability of the STR[22,23], underpinning that p is linked to the likelihood of STR slippage (**Fig 1g**). Similarly, upon introduction of the DivisionRecorder into immortalized embryonic fibroblasts from the Ai9 mouse strain—that carry an endogenous lox-STOP-lox-RFP cassette[24]—a low and predictable DR^{RFP} acquisition was observed, with a [G]33 STR conferring a p of 0.0052 ±0.00074 (**Fig. 1h, i**), thereby enabling the measurement of replicative history over many cell divisions (in theory >1,500 population doublings, **Fig. 1d**).

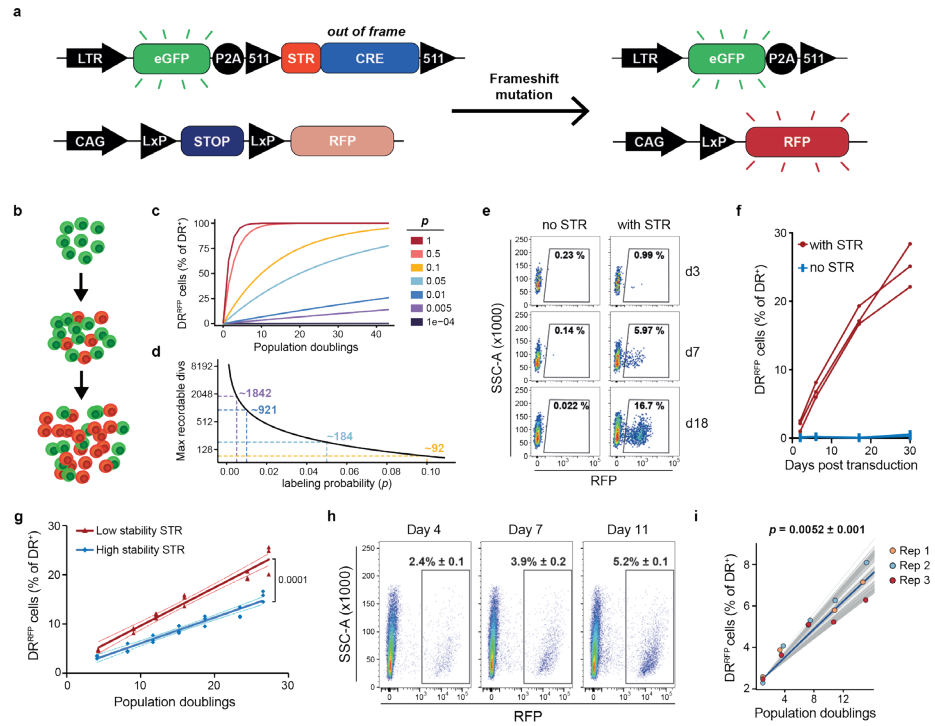

Fig. 1. DivisionRecorder activation is a proxy for replicative history. a, Schematic overview of the DivisionRecorder system. **b,** Cartoon depicting progressive DivisionRecorder activation in a proliferating cell pool. **c,** Simulation of the minimal ODE model (See **Supplementary Note 2** for detailed description and equations), depicting DR^{RFP} acquisition as a function of population doublings for the indicated values of DR^{RFP} acquisition probability (p). **d,** Maximal number of theoretically recordable population doublings, approximated by calculating the amount of division events required to reach a 99% DR^{RFP} population. Approximate maximums for selected values of p are indicated, colors correspond to legend in panel c. **e-f,** Percentage of DR^{RFP} cells over time in cultured $DivisionRecorder^+$ (DR^+) CRE-activity reporter HEK 293T cells (n=3 replicates per group) in which the CRE recombinase gene was preceded by either a stable nucleotide region (indicated as "no STR") or a repeat of 24 guanines (indicated as "with STR"). Representative plots (**e**) and summarizing line graphs (**f**) are shown. Lines connect experimental replicates **g**, Percentage of DR^{RFP} cells across population doublings in DR^+ CRE-activity reporter HEK 293T cells (n=3 replicates per group) in which the CRE recombinase gene was preceded by either a low stability STR ([G]24) or a high stability STR ([CA]30). Dots indicate individual samples, lines represent fitted linear regression, dotted lines indicate bounds of the 95% confidence interval. **h-i,** Percentage of DR^{RFP} cells across population doublings in immortalized DR^+ mouse embryonic fibroblasts. Representative flow cytometry plots (**h**) and summarizing graph (**i**) are shown. Best fits of the minimal ODE model are depicted (100 bootstraps per experimental replicate, **Supplementary Note 2**). Blue line represents the median of the bootstraps, grey lines represent individual fits, dots indicate experimental measurements (n=3 replicates). p indicates the estimated DR^{RFP} acquisition probability. Depicted experimental data are representative of at least two independent experiments. P values (**g**) were determined by two-sided ANCOVA test.

To test whether the DivisionRecorder can be used as a proxy for replicative history in the CD8⁺ T cell compartment in vivo, we generated Ai9;OT-I mice, in which all T cells recognize the $OVA_{257-264}$ epitope, thereby allowing examination of T cell pools in the context of equal TCR affinity. Ai9;OT-I T cells were isolated, modified with the DivisionRecorder to obtain DR⁺ OT-I T cells, transferred into *Listeria monocytogenes*-OVA (*Lm*-OVA) infected mice, and the fraction DR^{RFP} cells was measured over time (**Fig. 2a**). At early time-points post cell transfer (d1-d4), a rapid increase in DR^{RFP} cells was observed (**Fig. 2b, c**), coinciding with the proliferative burst of the antigen-specific CD8⁺ T cell pool. To determine whether the observed accumulation of DR^{RFP} cells formed an accurate measure of prior cell division, DR⁺ OT-I T cells were stained with CellTrace Violet (CTV) prior to cell transfer. Notably, analysis of the fraction DR^{RFP} cells within cell pools with different degrees of CTV dilution revealed a close correlation (**Fig. 2d, e**, $r_{rm} = 0.94$), providing direct evidence that in vivo DR^{RFP} acquisition reflects the extent of past division in the CD8⁺ T cell pool. In conclusion, these data establish that the DivisionRecorder allows the long-term measurement of division history in cell pools in vivo, in a way that is compatible with down-stream methodologies such as single cell sequencing (see below).

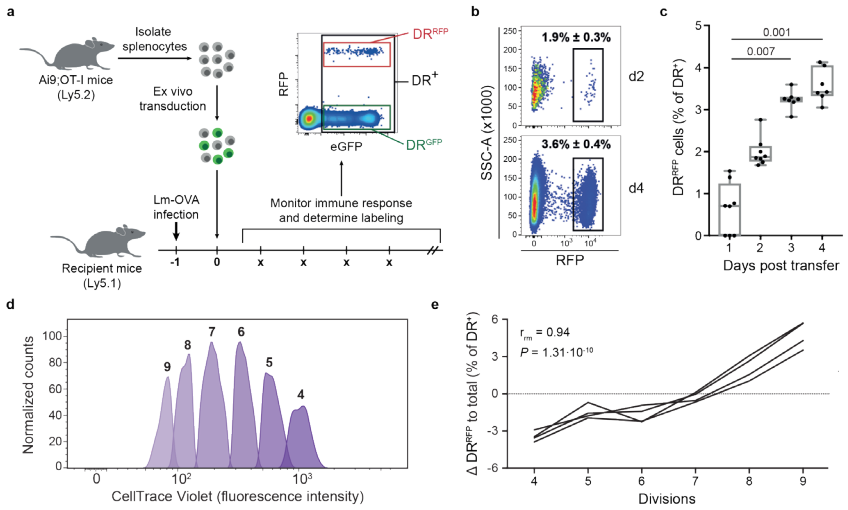

Fig. 2. The DivisionRecorder can be applied to study T cell division kinetics in vivo. a, Overview of experimental setup. **b-c,** DR⁺ OT-I T cells were transferred into recipient mice 24 hours post infection with *Lm*-OVA. Spleen samples were analyzed for the percentage of DR^{RFP} cells at day 1-4 post cell transfer. Representative pseudo-color density plots (**b**), and boxplots (**c**) in which the boxes indicate group median and 25th/75th percentiles, whiskers represent min/max, dots represent individual samples (n=8 mice for day 1 and 2; n=7 mice for day 3 and 4). **d-e,** CTV-stained OT-I T cells were retrovirally transduced with the DivisionRecorder and transferred into recipient mice (n=4) 24 hours post infection with *Lm*-OVA. 48 hours post-transfer, splenic DR⁺ OT-I T cells were assessed for CTV dilution (**d**), and the percentage of DR^{RFP} cells within each division peak was analyzed (**e**). All depicted data are representative of at least two independent experiments, lines and symbols indicate individual mice or samples. *P* values were determined by two-sided Kruskal-Wallis test, with Dunn's multiple comparisons test (**c**), or two-sided repeated measurement correlation test (**e**).

CD8⁺ T_{CM} cells are derived from replicative mature T cells.

Having validated the utility of the DivisionRecorder to record T cell division, we next sought to determine the replicative history of the total CD8⁺ T_M pool relative to that of the T_{EFF} pool. Analysis of the size of the DR⁺ OT-I T cell compartment in blood following *Lm*-OVA infection showed the characteristic rapid expansion phase, with T cell numbers peaking around day 6, and subsequent contraction into a stable memory pool (**Fig. 3a**). Notably, DR^{RFP} cells remained detectable following formation of T cell memory, thus allowing analysis of replicative history at late time points after infection (**Fig. 3b**).

In case T_M would primarily be derived from T cells that had undergone limited proliferation upon primary antigen encounter, the fraction of DR^{RFP} cells would be expected to decay during the contraction phase, due to the decline in the number of clonally expanded T_{EFF} (**Extended Data Fig. 1, Supplementary Note 3**). However, analysis of DR^{RFP} frequencies in blood demonstrated that the fraction of DR^{RFP} cells did not decline, but instead continued to increase during contraction and memory phase (an increase of 2.07% ±0.77% between day 13 and 59, **Fig. 3c**). This increase in DR^{RFP} frequencies post pathogen-clearance was not restricted to T cell responses induced by *Lm*-OVA infection, but was also observed upon infection with LCMV-OVA[25] (**Fig. 3d**), and was not due to anatomical redistribution of cells with distinct division histories, as the fraction of DR^{RFP} cells increased concurrently in peripheral blood and the primary sites of *Lm*-OVA infection (spleen/liver; **Fig. 3e, f**). Thus, in line with work by Akondy *et al.*[7], our results support the notion of a replicative 'mature', rather than 'nascent', CD8⁺ T_M pool, and extends this observation beyond the peripheral blood compartment to the sites of infection.

It has been well documented that T_{CM} are able to maintain the memory pool through infrequent homeostatic cell division[15,26,27], and recent work has shown that precursor-T_{CM} slow down their replicative cycle early during the expansion phase[10], suggesting limited clonal expansion of these cells during the early phase of the T cell response. However, it is difficult to translate cell-cycle activity at a given time-point into cumulative proliferative history, and we therefore wished to directly test the relationship between cell state (e.g., T_{CM} or T_{EM}) and replicative history during different stages of the T cell response. To this end, the fraction of DR^{RFP} cells within the T_M pool was calculated at varying expression levels of proteins associated with either multipotency or terminal differentiation (**Fig. 3g**). This analysis revealed a positive correlation between replicative history and the expression of the T_{CM}-associated proteins CD27 ($r_{rm} = 0.81$, $P = 6.2{\cdot}10^{-14}$) and CD62L ($r_{rm} = 0.62$, $P = 5.6{\cdot}10^{-7}$)[15,28,29], and a negative relationship between prior division and the expression of the T_{EM}-associated proteins KLRG1 ($r_{rm} = -0.83$, $P = 9.0{\cdot}10^{-15}$) and CX_3CR1 ($r_{rm} = -0.75$, $P = 4.5{\cdot}10^{-11}$)[14,15,30]. Likewise, defining multipotent T_{CM} and terminally differentiated T_{EM} subsets by joint expression or absence of CD62L and CD27, respectively, (**Extended Data Fig. 2a**), and further partitioning based on the expression of KLRG1 or CX_3CR1, revealed a positive association between division history and a less

differentiated cell state (**Extended Data Fig. 2b**). Furthermore, the division history of CD27^{HI}KLRG1^{LO} T_{CM} present in lymph nodes equaled that of T_{CM} in the spleen, implying that division history is dictated by cell state rather than anatomical location (**Extended Data Fig. 2c**).

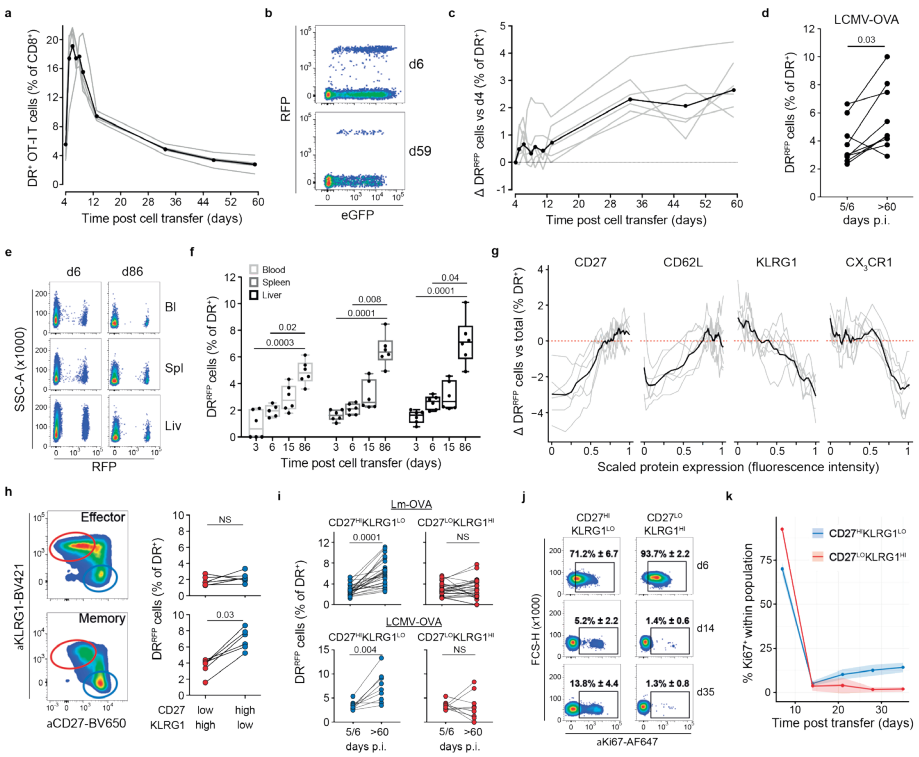

Fig. 3. The multipotent memory T cell pool is formed by replicative 'mature' cells. a-c, Kinetics of DR$^+$ OT-I T cells (**a**) and the percentage of DR^{RFP} relative to day 4 (**c**) in response to *Lm*-OVA, measured in peripheral blood (n=6 mice). Representative flow cytometry plots (**b**) showing DR^{RFP} and DR^{GFP} frequencies at indicated time points, and line graphs (**a, c**) depicting kinetics of single mice (grey) and group median (black). **d,** DR^{RFP} percentages within blood at day 5/6 (T_{EFF}) and day >60 (T_M) following LCMV-OVA infection (n=7). **e,** Representative plots depicting DR^{RFP} frequencies in blood (Bl), spleen (Spl) and liver (Liv). **f,** Percentage of DR^{RFP} detected in indicated organs of recipient mice at the indicated time points (n=6 mice per time point; response to *Lm*-OVA). Boxplots indicate group median and 25th/75th percentiles, whiskers represent min/max, dots represent individual samples. **g,** Moving average of surface marker expression level on splenic DR$^+$ cells plotted against the percentage of DR^{RFP} within each window during memory (day 86; n=6), means are shown in black. DR^{RFP} percentages within each window are corrected for the total percentage of DR^{RFP} detected in that sample. **h,** Gating strategy (left) and DR^{RFP} percentages (right) of CD27^{HI}KLRG1^{LO} and CD27^{LO}KLRG1^{HI} cells in spleen during effector (d6, top) and memory phase (d86, bottom; n=6) in response to *Lm*-OVA. **i,** DR^{RFP} percentages within the CD27^{HI}KLRG1^{LO} and CD27^{LO}KLRG1^{HI} cell populations in blood, comparing effector (day 5/6) and memory (day >60) phases. Data shown for *Lm*-OVA (top; n=22) and LCMV-OVA (bottom; n=7) infections. Lines connect individual mice. **j-k,** Ki67 expression by CD27^{HI}KLRG1^{LO} and CD27^{LO}KLRG1^{HI} OT-I cells in blood in response to *Lm*-OVA. Representative flow cytometry plot (**j**), and line graphs (**k**) where solid lines indicate population means, shaded areas indicate 95% confidence interval (n=11 mice).

Data shown for *Lm*-OVA (top; n=22) and LCMV-OVA (bottom; n=7) infections. Lines connect individual mice. **j-k,** Ki67 expression by CD27^{HI}KLRG1^{LO} and CD27^{LO}KLRG1^{HI} OT-I cells in blood in response to *Lm*-OVA. Representative flow cytometry plot (**j**), and line graphs (**k**) where solid lines indicate population means, shaded areas indicate 95% confidence interval (n=11 mice). All depicted data are representative of at least two independent experiments, lines and symbols indicate individual mice or samples. *P* values were determined by two-sided Kruskal-Wallis test with Dunn's multiple comparisons test (**f**), or two-sided Wilcoxon's signed-rank test (**d, h, i**).

Next, to delineate at which point the divergence in replicative history between T cells with a T_{CM}-like multipotent and T_{EM}-like terminally differentiated phenotype developed, we assessed the link between phenotypic marker expression and DR^{RFP} fractions throughout the T cell response. Notably, replicative history varied minimally across T_{EFF} cell states at the peak of the antigen-specific T cell response (d6 post transfer, **Fig. 3h, Extended Data Fig. 2d-f**), followed by selective accumulation of DR^{RFP} within the CD27^{HI}KLRG1^{LO} early-T_{CM} pool directly after the peak of the expansion phase (**Fig. 3h, i, Extended Data Fig. 1g**), due to continued replicative activity of this subset (**Fig. 3j, k**). The observation that the division history of CD27^{LO}KLRG1^{HI} T cells stays constant post effector phase (**Fig. 3i**) suggests that, in addition to the previously documented lack of proliferative activity of this cell pool[15,26,31], this terminally differentiated subset also does not receive significant replenishment by the replicative active CD27^{HI}KLRG1^{LO} T cell pool (**Extended Data Fig. 1h**). The substantial number of divisions that we observe in the CD27^{HI}KLRG1^{LO} cell pool at the peak of the response appears at odds with the proposed limited clonal expansion of precursor-T_M. However, these observations may either be reconciled by the reported trans-differentiation between T_{EFF} cell states[14,15,30], or by the fact that a reduced proliferative activity may form a property of only a small part of the memory precursor pool[10,11,32]. In summary, the above data indicate that the high amount of prior division of the T_{CM} pool results from both strong proliferative activity during the effector phase and selective proliferative activity after pathogen clearance.

Replicative history identifies distinct T_{CM} cell states.

Increasing evidence suggests that the T_{CM} pool is highly heterogeneous in terms of both gene expression profiles and prior and ongoing replicative behavior[14,15,33], providing an incentive to test for possible associations between division history and transcriptional states within this cell pool. To this end, we carried out single-cell mRNA sequencing (scRNAseq) on DR^{GFP} and DR^{RFP} memory OT-I T cells (75-85 days post *Lm*-OVA infection; **Extended Data Fig. 3**). In addition, to test whether DR$^+$ OT-I T_M assume the same spectrum of transcriptional states as non-modified T cells, we performed scRNAseq on OT-I T_M that were generated through adoptive transfer of a small number (2,000) of naïve OT-I T cells followed by *Lm*-OVA infection 24 hours later. DR$^+$ OT-I and unmodified OT-I memory T cells were jointly grouped into 23 transcriptionally distinct MetaCells (MCs)[34] that included 4 T_{EM} and 19 T_{CM} MCs based on the expression of a small set of multipotency- and effector-associated genes (**Fig. 4a,b**). Notably, while memory T cells derived from small numbers of unmodified OT-I T cells showed a proportionally

greater contribution to T_{EM} MCs—consistent with the relationship between precursor frequency and T_{EM} formation[35]—DR$^+$ OT-I T cells and unmodified OT-I T cells were equal in their potential to yield the 19 distinct T_{CM} MCs (**Extended Data Fig. 4**), indicating that the introduction of the DivisionRecorder did not measurably impact the ability of T cells to differentiate into different T_{CM} states.

Amongst the observed T_{CM} MCs, two transcriptionally distinct subgroups could be identified (**Fig. 4b**). Specifically, while all T_{CM} showed the expected high expression of *Bcl2*, *Sell and Cd27,* and minimal expression of *Cx3cr1*, *Zeb2, Gzma and Prdm1* (**Fig. 4c, Extended Data Fig. 5a**), a dichotomy was observed in the expression of multipotency-associated (e.g. *Myb*, *Ccr7*) and effector-associated (e.g. *Tbx21*, *Lgals1*) genes within the T_{CM} pool (denoted as T_{CM}(mult) and T_{CM}(eff), respectively in the figures; **Fig. 4b, Extended Data Fig. 5a**). Next, we assessed the relation between transcriptional state and replicative history within the memory T cell pool. In line with the flow cytometry data, the replicative history of T_{CM}—as a whole—exceeded that of T_{EM}, thereby validating the scRNAseq approach. Strikingly, T_{CM} enriched for effector genes had overall higher DR^{RFP}/DR^{GFP} ratios compared to T_{CM} enriched for multipotency genes, demonstrating that stemness-related transcriptomic features are inversely associated with division history within the T_{CM} pool (**Fig. 4d**). Correspondingly, comparison of the three T_{CM} MCs with the highest and lowest level of prior division (hdT_{CM} and ldT_{CM}, respectively) revealed that ldT_{CM} were marked by the expression of key multipotency-associated genes, including *Tcf7*, *Sell, Myb and Eomes*, and several survival factors (*Gimap* and *Birc* family members, **Extended Data Fig. 5b, c**). Moreover, one ldT_{CM} MC was highly enriched for transcripts involved in inhibitory function (*Lag3*, *Cd160*, *Tox*), suggesting a possible analogy with the inhibitory signaling-dependent T_{CM}-precursor subset identified by Johnnidis *et al.*[33] (**Extended Data Fig. 5c**). In contrast, hdT_{CM} commonly expressed genes related to terminal differentiation, such as *Lgals1* and *S100* family members, and showed increased transcript levels for cytotoxicity-associated genes (*Nkg7*, *Ctsw*; **Extended Data Fig. 5b, c**). This link between replicative history and a multipotency versus effector-associated gene expression signature within the T_{CM} pool was further validated by differential gene expression analysis and gene set enrichment analysis (**Fig. 4e-g, Extended Data Fig. 5d**). In line with this association, *ex vivo* antigen stimulation of T_{CM} harvested from *Lm*-OVA memory mice showed that T_{CM} that had undergone more prior divisions were more likely to degranulate and less likely to produce IL-2, as compared to their less divided T_{CM} counterparts (**Extended Data Fig. 5e, f**).

The observed divergence in replicative history between distinct T_{CM} states potentially reflects the selective quiescence of a subset of T_{CM} with a less differentiated state. Of note, ldT_{CM} showed reduced expression of Myc targets and genes involved in cell metabolism (**Extended Data Fig. 5g**), suggesting that these cells exist in a transcriptionally-enforced replicative quiescent state. To test for such a transcriptional state, we scored the expression of a core gene set of quiescent stem cells from various tissues[36] (hereafter referred as

QstemScore). Notably, T_{CM} that showed increased expression of multipotency-associated genes were marked by a higher QstemScore than T_{CM} with increased expression of effector-associated genes. (**Fig. 4h**).

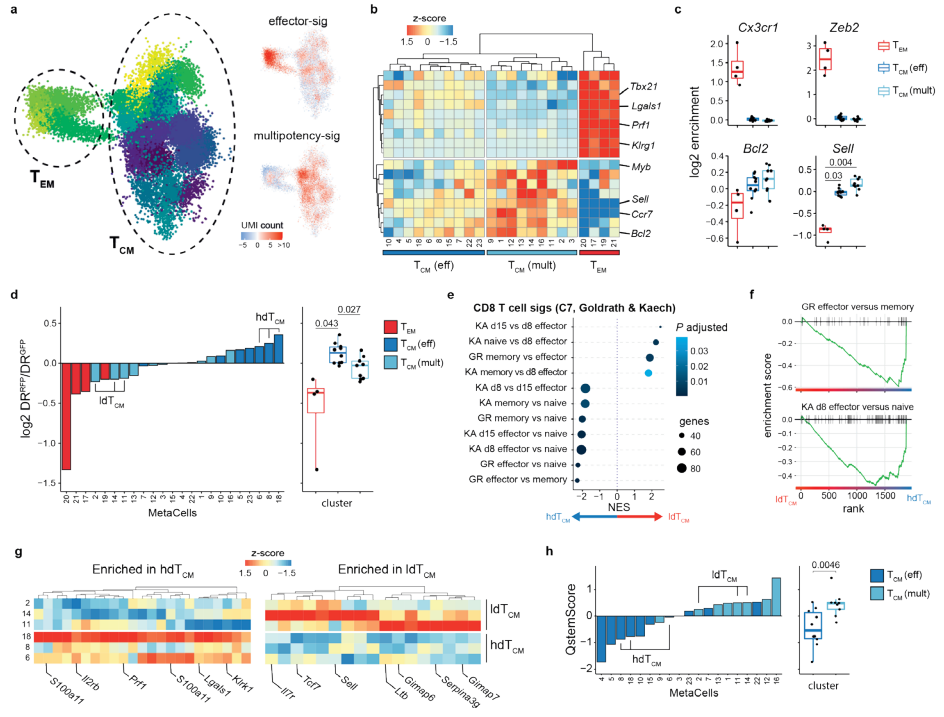

Fig. 4 Replicative history identifies distinct transcriptional states within the T_{CM} pool. Single cell transcriptomic profiling of DR$^+$ T cells obtained from spleen in memory phase (Day 75 and 85 post *Lm*-OVA infection)**. a,** 2D projection of all profiled cells, colors indicate MCs (left), or relative expression of effector- and multipotency-associated genes (right). Gene list in **Supplementary Table 1**. **b,** Hierarchical clustering of MCs by their expression of effector- and multipotency-associated genes used in A. MCs are divided into 3 clusters based on Euclidean distance. **c,** Expression of selected genes by each MC cluster. **d,** DR^{RFP}/DR^{GFP} ratio within each MC, depicted as waterfall plot (left) and boxplot (right). **e-f,** Enrichment of gene signatures from MSigDB (C7, collections deposited by Goldrath (GR) and Kaech (KA), **Supplementary Table 2**) by gene set enrichment analysis comparing ldT_{CM} and hdT_{CM} (**e**), and enrichment plots (**f**) of 2 representative gene sets. **g,** Heatmaps depicting genes involved in immune function that were significantly ($P < 0.05$) depleted (left) or enriched (right) within ldT_{CM} (See **Extended Data Figure 4d**, **Supplementary Table 3**). Selected genes are annotated, complete gene lists in **Supplementary Table 4**. **h,** QstemScore of all T_{CM} MCs depicted as waterfall plot (left) and boxplot (right). QstemScore is based on marker genes of quiescent stem cells (**Supplementary Table 5**)[30], see methods for calculation. Data depicted were accumulated in two independent experiments (3-4 mice per experiment). Boxplots (**c, d, h**) indicate group median and 25th/75th percentiles, whiskers indicate the interquartile range multiplied by 1.5, dots signify individual MCs. The phenotype clusters T_{EM}, T_{CM}(eff) and T_{CM}(mult) contain 4, 9 and 10 MCs, respectively. *P* values were determined by two-sided Tukey's HSD test (**c**), two-sided Student's T test with false-discovery rate correction (**d, h**), the FGSEA algorithm followed by the Benjamini-Hochberg procedure (**e**), or two-sided Wilcoxon Rank Sum test with Bonferroni correction (**g**). Significant *P* values (< 0.05) are indicated in the plots.

Moreover, variation in QstemScore could also be detected in gp33-specific P14 T_{CM} from an external data-set[37], and those P14 T_{CM} that prominently expressed this gene set transcriptionally resembled the multipotency-signature^{HI}, effector-signature^{LO} OT-I ldT_{CM} described here (**Extended Data Fig. 6**). Together, these data suggest a link between T_{CM} quiescence and the expression of multipotency-associated genes, driving the divergence in replicative history between distinct T_{CM} states.

To directly test whether replicative behavior in the T_{CM} pool is associated with a multipotency-associated state and relates to the functional capacity of T_{CM} to re-expand upon secondary activation, we established a DivisionRecorder-independent, CTV-based serial-transfer approach (**Fig. 5a**). Naïve OT-I and GFP;OT-I T cells were transferred into primary recipients that were subsequently exposed to *Lm*-OVA infection. At day 30 post-infection, early memory T cells were harvested, CTV labeled and transferred into infection-matched secondary recipients. 75 days later, CTV^{HI} (div0-2) and CTV^{LO} (div5+) T_{CM} were isolated, and the resulting T_{CM} populations were then profiled by scRNAseq, or transferred at a 1:1 ratio into tertiary recipients that were subsequently challenged with *Lm*-OVA. Strikingly, comparison of quiescent (div0-2) cells and proliferative (div5+) T_{CM} by gene set enrichment analysis revealed a clear negative association between quiescence and an effector-like transcriptional state, while quiescence was positively associated with multipotency-associated gene expression (**Fig. 5b, c, Extended Data Fig. 7a**). Likewise, inspection of MCs (**Extended Data Fig. 7b-e**) that were enriched in the div0-2 cells, showed a prominent expression of multipotency-associated genes (*Myb*, *Tcf7*, *Id3)*, whereas those enriched in div5+ cells showed increased expression of effector-associated genes (*Id2*, *S00a4*, *Lgals1*) (**Fig. 5d, e**). Furthermore, comparison of the expansion potential of div0-2 and div5+ T_{CM} demonstrated that quiescent T_{CM} were superior in generating offspring upon renewed infection (**Fig. 5f, g**), further demonstrating that replicative heterogeneity in the T_{CM} pool is both linked to transcriptional state and functionality.

Re-expansion potential of T_{CM} is linked to prior division.

Having observed a link between prior division and recall potential in adoptive transfer experiments, we set out to verify this relationship without disruption of the T_M niche, through re-challenge of recipient mice carrying DR$^+$ memory OT-I T cells. In case the capacity for renewed expansion would primarily be restricted to replicative quiescent T_{CM} cells, the fraction of DR^{RFP} cells should show an initial decay upon reinfection—due to the increased preponderance of offspring derived from this previously quiescent population—followed by a gradual recovery throughout the contraction phase, as a result of novel division-dependent label acquisition. Notably, analysis of the fraction of DR^{RFP} T cells in blood revealed a steep decline during the first days post-secondary infection, followed by a gradual recovery during secondary memory formation (**Fig. 6a**, **Supplementary Note 4**). This transient reduction in the DR^{RFP} fraction was observed in multiple anatomical compartments (blood, spleen, liver), occurred independent of

cell phenotype, and was also observed in LCMV-OVA induced T_M pools responding to secondary challenge (**Fig. 6b-d**). Of note, DR^{RFP} cell accumulation during the secondary contraction phase occurred at a comparable rate as during the primary response (**Fig. 6e**), yielding a secondary T_M pool that—despite extensive renewed clonal expansion—had undergone a similar number of divisions as the initial memory pool (**Fig. 6f,** median fold difference = 1.03). Thus, the replicative histories of the T_{EFF} and T_M pools of the secondary T cell response mimic those of the primary T cell response, supporting the notion that the secondary expansion wave is mounted by a group of T_{CM} that has undergone limited prior division. Furthermore, this low-division T_{CM} pool is able to repeatedly reconstitute the effector T cell pool, as the same decrease in the fraction of DR^{RFP} cells was observed upon tertiary infection of mice (**Fig. 6g**).

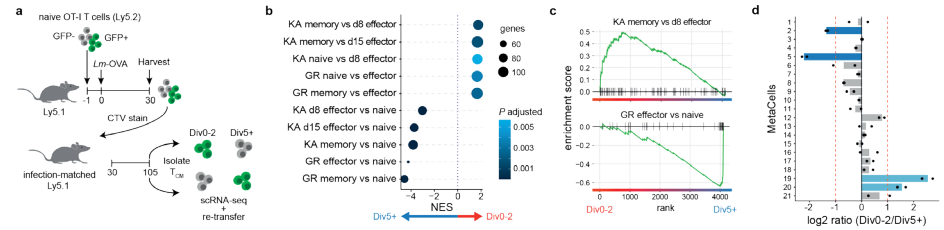

Fig. 5 Replicative history is linked to recall-potential within the T_{CM} pool. a, Experimental setup. Primary recipient mice received 5·10^5 naïve OT-I and 5·10^5 naïve GFP;OT-I T cells. 30 days after *Lm*-OVA challenge, CD8 T cells were enriched, labelled with CTV and transferred into infection-matched secondary recipient mice (1 primary recipient per secondary recipient). At d105 post infection, splenic CD27$^+$KLRG1$^-$ memory T cells that had either divided 0-2 or 5+ times and were either GFP$^+$ or GFP- were isolated by FACS. **b,** Enrichment of gene signatures from MsigDB (C7, collections deposited by Goldrath (GR) and Kaech (KA), **Supplementary Table 2**) between Div0-2 and Div5+ cells. Top and bottom 5 pathways are depicted. **c,** Enrichment plots of representative pathways detected in by gene set enrichment analysis. **d,** Ratio of normalized counts between Div0-2 and Div5+ cells within each MC separately calculated for GFP$^+$ and GFP$^-$ populations. Bars indicate averages, dots indicate ratios of either GFP$^+$ or GFP$^-$ OT-I T cells. Red dotted lines indicate a fold change of 2. **e,** Waterfall plots depicting top and bottom 6 marker genes for selected MCs, filtered for genes involved in immune function (**Supplementary Table 3**). **f,** Flow cytometry plots depicting pre-transfer mixes of Div0-2 and Div5+ T_{CM}. **g,** 8,000-12,000 total memory T cells as described in **f** were transferred into infection-naïve mice, following *Lm*-OVA challenge 24 hours later. Ratios between Div0-2 and Div5+ derived cells was determined from peripheral blood samples at indicated days post infection. Lines connect populations from individual mice (Experiment 1 n = 3; Experiment 2 n = 5). Depicted scRNAseq data was collected from 4 mice, data describing recall potential was obtained from 8 mice. *P* values were determined by the FGSEA algorithm followed by the Benjamini-Hochberg procedure (**e**).

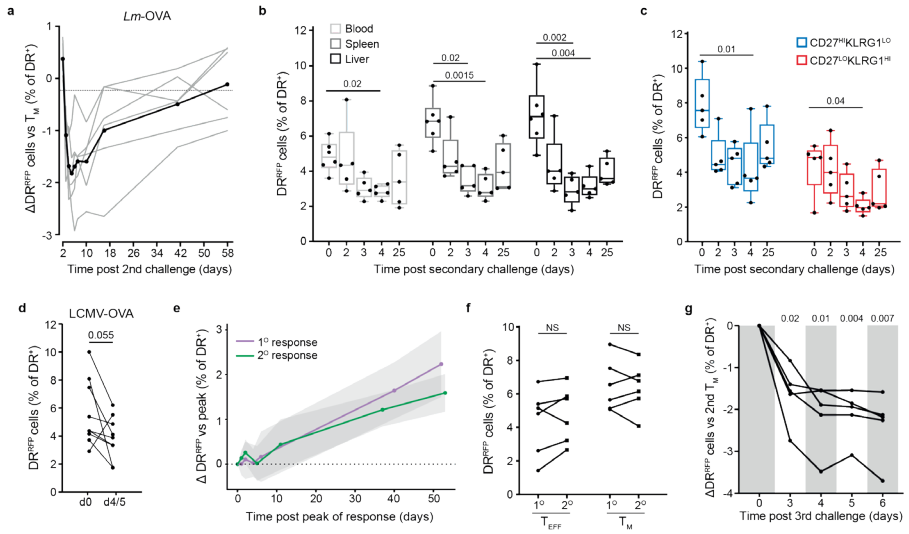

Fig. 6. The secondary T_{EFF} pool is predominantly generated by previously quiescent memory T cells. a, Kinetics of the percentage of DR^{RFP} cells in blood upon secondary *Lm*-OVA infection. Values are relative to the DR^{RFP} percentage within the respective memory pools (n=6 mice), black line represents group mean. **b-c,** DR^{RFP} percentages in indicated organs (**b**), or within splenic $CD27^{LO}KLRG1^{HI}$ and $CD27^{HI}KLRG1^{LO}$ populations (**c**) at indicated time points (n=6 mice per time point) post-secondary infection. Boxplots indicate group median and 25th/75th percentiles, whiskers represent min/max, dots represent individual samples. **d,** DR^{RFP} percentages in blood at memory (day >60) and at the peak of the secondary response (day 4/5 post-recall). Memory pools were generated with LCMV-OVA, recall infection was performed with *Lm*-OVA. **e,** DR^{RFP} acquisition in blood following primary and secondary infection. Values are relative to DR^{RFP} percentage at the peak of the primary or secondary response. Lines represent group medians (n=6 mice per group), greyed areas represent 95% confidence intervals. **f,** DR^{RFP} percentages in blood during effector and memory phases of the primary and secondary responses. Lines connect data of individual mice (n=6). **g,** DR^{RFP} percentages in blood (n=5 mice) upon tertiary infection. Mice were challenged twice with *Lm*-OVA with a >60 days interval, and subsequently infected with LCMV-OVA >60 days post-secondary infection. Depicted data are representative of at least 2 independent experiments. *P* values were determined by two-sided Kruskal-Wallis test with Dunn's multiple comparisons test (**b, c**), two-sided Wilcoxon signed-rank test (**d, f**), or repeated-measures one-way ANOVA followed by Dunnett correction (**g**).

To determine whether the observed data are consistent with re-expansion being driven by a memory T cell subset that becomes quiescent early in the immune response, we simulated T cell responses in which a fraction of T_{CM} precursors acquires replicative quiescence during the primary T cell response (see **Supplementary Note 5, Extended Data Fig. 8a**). Specifically, T cell responses were simulated that yielded quiescent T cells at a frequency of either ~0.1% or ~1% of the T_{EFF} pool, resulting in T_M pools in which quiescent T_{CM} accounted for ~3 and ~25 percent of the memory population (**Fig. 7a**). Modeling of DR^{RFP} labeling rates during recall responses in which the potential to re-expand was either abruptly lost as a function of the number of prior divisions (fun 1 and 2), or was lost more gradually across division history (fun 3), demonstrated that the transient drop in DR^{RFP} fractions is only consistent with models in which the capacity

to re-expand is restricted to cells that have undergone limited clonal expansion (**Fig. 7a, b**). Furthermore, the stringency of this relation is strongly dependent on the relative size of the quiescent T_{CM} pool (**Fig. 7b**).

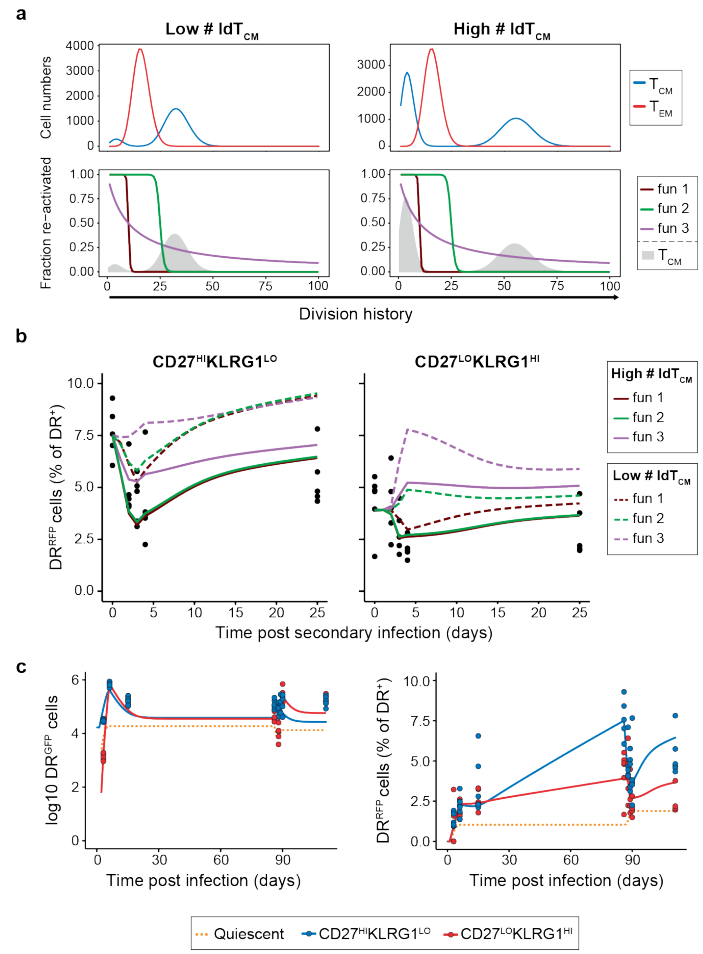

Fig. 7. Modelled T cell responses are consistent with the presence of a replication-competent quiescent T_{CM} population. a, Division history of T_{CM} and T_{EM} pools generated by modelled T cell responses (see **Supplementary Note 5**) during which a high (capped at 1% of the T_{EFF} pool size) or low (capped at 0.1% of the T_{EFF} pool size) fraction of T cells acquire quiescence during the effector phase (top). 3 re-expansion functions were used to restrict which fraction of T_{CM} with a given number of prior divisions will re-expand during recall (bottom). For reference, the division history of T_{CM} is shown as a shaded area. **b,** Modelled DR^{RFP} percentages within the $CD27^{LO}KLRG1^{HI}$ and $CD27^{HI}KLRG1^{LO}$ populations during secondary responses, with each re-expansion function applied to a memory pool containing either a high or low number of quiescent T_{CM}. Black dots indicate experimental measurements. **j,** Best fit of the modelled T cell response (number of quiescent T cells capped to 1% of T_{EFF}) experimental data obtained from spleen, depicting either cell numbers (left) or DR^{RFP} percentages (right). See **Supplementary Note 5** for details. Lines indicate the modeled populations; dots indicate experimental measurements.

Taken together, our data establish that replicative state is not homogeneously distributed within the T_{CM} pool and is linked to distinct transcriptional and functional properties. Specifically, our observations are consistent with a dichotomy in the T_{CM} pool, in which a self-renewing T_{CM} population maintains the T_M pool but marginally contributes to secondary expansion, and a replication-competent quiescent T_{CM} population is required to form the T_{EFF} pool that arises upon renewed infection (**Fig. 7c, Extended Data Fig. 8, 9**).

DISCUSSION

Here, we report the development and application of the DivisionRecorder to dissect the replicative history of cell pools *in vivo*. We show that this approach allows longitudinal examination of division history, and how it may be combined with technologies such as flow cytometry and scRNAseq to couple cell state to division history. In the application presented here, the DivisionRecorder requires viral transduction to introduce one of its modules. While this did not significantly disrupt cell behavior in our study, development of a fully germline encoded DivisionRecorder system will be attractive, for instance, to follow replicative behavior of cell pools that are not amenable to adoptive transfer.

Using the DivisionRecorder, we demonstrate that, as a whole, the multipotent CD8$^+$ T cell pool has undergone substantial proliferation at the peak of the expansion phase, and continues to proliferate following pathogen clearance, resulting in a cumulative replicative age of the T_{CM} pool that exceeds that of the T_{EFF} and T_{EM} pool. Previous work has shown that a fraction of CD62L^{HI} precursor-T_M divide at a lower rate than terminally differentiated effector subsets[10,11,32]. In line with this, we observed a lower fraction of Ki67^{HI} cells within the multipotent effector pool compared to the terminally differentiated pool, early post infection. At the same time, our data indicate that this difference does not result in a reduced cumulative number of past divisions within the entire CD62L^{HI} T_{EFF} pool. Conceivably, these findings may be reconciled by the ability of highly proliferative CD62L^{LO} T_{EFF} to phenotypically convert to a less differentiated CD62L^{HI} state[14,15,30]. Alternatively, the precursor-T_{CM} pool may harbor a heterogeneity in replicative history that is not revealed by the phenotypic markers used.

In line with the latter possibility, by combining the DivisionRecorder with scRNAseq we reveal that, while the T_{CM} pool has undergone substantial prior division as a whole, replicative history is heterogeneous within this pool and is associated with specific transcriptional states. First, our data demonstrate the presence of T_{CM} that bear transcriptional similarities to T_{EM} cells but, in contrast to T_{EM}, remain highly proliferative in the absence of inflammation (**Extended Data Fig. 9**). Second, we identify a population of quiescent T_{CM} that expresses reduced levels of effector-associated genes, and high levels of pro-survival genes and genes associated with quiescent stem cells[36]. Several recent studies have reported the early emergence of TCF-1^{HI} and CD62L^{HI} effector cells that

develop into memory T cells exhibiting stemness features[38,39]. Moreover, Johnnidis *et al.*[33] propose early expression of inhibitory receptors as a mechanism preserving hallmark memory features. Although these early T cell subsets bear similarities to the quiescent T_{CM} observed here, further investigations into the developmental origin of distinct T_{CM} states are necessary to better understand the lineage relationships between the T_{CM} states described here, and those present during the early phases of the T cell response.

A hallmark of immunological memory is the ability to efficiently generate a new wave of T_{EFF} upon renewed infection. Our data demonstrate that this ability is predominantly confined to a subgroup of replicative nascent T_M cells. The combined observations of a less differentiated quiescent T_{CM} population, and the reconstitution of the secondary and tertiary T_{EFF} pool by the output of these nascent progenitors, make a compelling argument for the presence of a bona fide stem cell population within the T_M pool. A growing body of work has examined a stem cell-like memory T cell (T_{SCM}) population[40,41], generally using cell phenotype to enrich and study these cells *ex vivo*. Using a function-driven, phenotype-agnostic, approach that does not require removal of cells from their niche, we observe a cell behavior that fits the profile of stem cell-like memory T cells *in situ*.

In high turnover tissues, such as the bone marrow[42,43], the intestinal epithelium[44,45] and skin epidermis[46,47], two distinct behaviors of multipotent progenitor cells have been described: Actively dividing cells that promote normal tissue homeostasis, and quiescent cells that have been documented to break their dormancy upon tissue injury and exhibit profound re-population capacity[42,45,48,49]. We propose that the two T_{CM} behaviors we describe provide the T cell compartment with the same capacity for renewal. Thus, the T cell pool can be viewed as an autonomous tissue that abides by organizing principles akin to those of the hematopoietic system and solid organs.

ACKNOWLEDGEMENTS

We would like to thank Monika C Wolkers (Sanquin, Amsterdam), Carmen Gerlach (Karolinska Institute, Stockholm) and Klaas van Gisbergen (Sanquin, Amsterdam) for helpful discussions regarding experimental procedures and sharing biological material, and Doron Merkler (University of Geneva, Geneva) for kindly providing the artLCMV-OVA. In addition, we would like to thank the NKI Genomics Core Facility and Flow Cytometry Core Facility for providing experimental support. This work was supported by ERC AdG Life-his-T (Grant agreement ID: 268733) to T.N.S. and an NWO grant (ALWOP.265) to R.J.d.B.

Author contributions

The study was designed by K.B., L.K., F.A.S. and T.N.S., and supervised by T.N.S. and F.A.S.; K.B. and L.K. jointly performed, analyzed, and visualized all experimental

work included in the manuscript; F.A.S and K.B designed and developed the retroviral DivsionRecorder construct. L.A.K. and L.J. performed optimization and validation experiments integral to the design of the DivisionRecorder; A.C.S and R.J.D.B. performed mathematical modelling, together with T.S.W, L.P and K.R.D; K.B. and L.K. wrote the manuscript with the input of co-authors; T.N.S. and F.A.S. critically reviewed and revised the manuscript.

Competing interests

The authors declare no competing financial interests.

METHODS

DivisionRecorder vector generation

In order to prevent expression of Cre recombinase during bacterial cloning, a synthetic intron—containing a splice donor, a branch site, a pyridine rich region, and a splice acceptor— was inserted into the Cre gene through three-fragment isothermal assembly. To prevent low level Cre translation occurring from alternative start sites, two ATG codons (position 78 and 84) were replaced by TGT codons. Finally, the Cre start codon was replaced by an EcoRI-spacer-XhoI site, to facilitate subsequent introduction of synthetic STRs. To generate the DivisionRecorder vector, two lox511 sites were introduced into the multiple cloning site of the pMX retroviral vector. Subsequently, an eGFP gene and the modified Cre recombinase gene were introduced directly upstream and downstream of the 5' lox511 site, respectively. Finally, a P2A element was inserted directly in between the eGFP gene and the 5' Lox511 site. Together, this resulted in a cassette comprising from 5' to 3': Kozak, an eGFP gene, a P2A site, a lox511 site, an EcoRI restriction site, spacer, an XhoI restriction site, a Cre recombinase gene, and a lox511 site. In its base configuration, Cre recombinase is out of frame. Synthetic STR domains were ordered as oligonucleotides (Invitrogen) and subsequently dimerized. STR dimers were inserted via the EcoRI and XhoI sites. Full sequences of all oligonucleotides are supplied in **Supplementary Table 6**.

Cre-activity reporter vector generation

LoxP sites were introduced into the multiple cloning site of the pCDH-CMVp-MCS-PGK-BlastR vector. In addition, a Katushka open reading frame was introduced, resulting in a vector containing from 5' to 3'; The CMV promoter, a floxed scrambled open reading frame, a Katushka open reading frame, the PGK promoter, and a blasticidin resistance gene.

Establishment of cell lines

The Cre-activity reporter cell line used in **Figure 1** was generated by retroviral transduction of HEK 293T cells (ATCC) with the Cre-activity reporter plasmid and subsequent Blasticidin selection (2 μg/ml, InvivoGen). Transduced cells were seeded at

1% confluency, and resulting single cell-derived colonies were transferred to individual wells. Clones were then examined for efficiency of induction of Katushka expression upon transfection with Cre recombinase, and the best-performing clone was selected. Cre-activity reporter cells were cultured in IMDM (Gibco) supplemented with 8% fetal calf serum (FCS, Sigma), 100 U/ml penicillin (Gibco), 100 μg/ml streptomycin (Gibco) and 2 mM Glutamax (Gibco). A mouse embryonic fibroblast (MEF) cell line from the Ai9 mouse strain was generated by modification of E14.5 embryonic fibroblasts with a retroviral vector encoding short-hairpin RNA directed against the p53 mRNA. Resultant cells were cultured in IMDM supplemented with 8% FCS, 100 U/ml penicillin, 100 μg/ml streptomycin and 2 mM Glutamax.

Mice

C57BL/6J-Ly5.1, OT-I, UBC-GFP and Ai9 mice were obtained from Jackson Laboratories, and strains were maintained in the animal department of The Netherlands Cancer Institute (NKI). Ai9 and OT-I, and UBC-GFP and OT-I mice were crossed to obtain the Ai9;OT-I and GFP;OT-I strains, respectively. Between 5-10 mice, both male and female, of the age of 6 to 15 weeks were used for each experiment. All animal experiments were approved by the Animal Welfare Committee of the NKI, in accordance with national guidelines.

Generation of DivisionRecorder⁺ OT-I T cells

Platinum-E cells (Cell Biolabs Inc) cultured in IMDM supplemented with 8% FCS, 100 U/ml penicillin, 100 μg/ml streptomycin, and 2 mM Glutamax were transfected with the DivisionRecorder vector using FuGene™6 (Promega). Retroviral supernatant was harvested 48h after transfection and stored at -80°C. Spleens from Ai9;OT-I mice were harvested and mashed through a 70 μm strainer (Falcon) into a single cell suspension and resulting splenocytes were subsequently treated with NH_4Cl to remove erythrocytes. Subsequently, splenocytes were cultured in T cell medium (RPMI (Gibco Life Technologies) with 8% FCS, 100 U/ml penicillin, 100 μg/ml streptomycin, Glutamax, 10mM HEPES (pH 7.4), MEM Non-Essential Amino Acids (Gibco), 1mM Sodium pyruvate (Gibco), 50 μM 2-mercaptoethanol, supplemented with 1 ng/ml recombinant murine IL-7 (PeproTech) and 2 μg/mL ConcanavalinA (Merck)). After 48h, splenocytes were re-seeded on RetroNectin (Takara) coated plates in T cell medium supplemented with 60 IU/mL human IL-2 and DivisionRecorder virus, and were centrifuged for 90min at 400g to allow spinfection. Virus concentration was chosen such that a transduction efficiency of approximately 10-15% was achieved, in order to minimize the occurrence of multiple retroviral integrations (**Supplementary Note 6**). Cells were harvested 24h later and a small aliquot was stained with anti-CD8-PercpCy5.5, anti-Vb5-PeCy7, anti-CD45.2-AF700 and DAPI to determine the fraction viable OT-I T cells ($DAPI^-CD8^+Vb5^+CD45.2^+$) by flow cytometry (Fortessa, BD Bioscience), which generally was around ~80%. $CD8^+Vb5^+CD45.2^+$ cells that expressed GFP were considered as DivisionRecorder⁺ OT-I cells. Within the initial population of DivisionRecorder⁺

OT-I cells, the fraction of cells that already showed reporter activation (as inferred by tdTomato expression) 24h after transduction was consistently between 0.4 and 0.8%. Activated splenocytes were prepared for adoptive transfer (see below).

Infection, adoptive transfer and cell recovery

C57BL/6J-Ly5.1 mice were infected with 5,000-10,000 CFU of a recombinant *Listeria monocytogenes* strain that expresses ovalbumin or with 5,000 PFU artLCMV-OVA[25]. Approximately 24h later, infected mice received 5,000-40,000 DivisionRecorder$^+$ OT-I T cells through intravenous tail vein injection. To analyze OT-I T cell responses in peripheral blood over time, 25-50 µL blood samples were obtained from the tail vein at the indicated time points, and were treated with NH_4Cl supplemented with 0.2 mg/ml grade-II DNaseI (Roche) to remove erythrocytes (see Methods, Flow Cytometry). To obtain spleen and liver samples, mice were sacrificed, organs were harvested, and single cell suspensions were prepared by means of mashing through a 100µM or 70µm strainer (Falcon), respectively. Subsequently, erythrocytes were removed by treatment with NH_4Cl. To purify leukocytes from single cell suspensions of liver tissue, cell suspensions were separated over a 37.5% Percoll (Sigma) density gradient. Obtained blood, spleen and liver samples were further processed for flow cytometric analysis, scRNA-sequencing or functional in vitro assays, as indicated. Samples were monitored for the occurrence of retroviral silencing; which was not observed in any of the examined samples (**Supplementary Note 7**)

Validation of DivisionRecorder functionality

To assess the ability of the DivisionRecorder to faithfully report on the replicative history of T cell populations using dilution of cell dyes as a reference, as described in **Fig. 2d-e**, we employed an experimental approach that was optimized to obtain sufficient DR^{RFP} events within the limited number of cell divisions that can be followed using cell dyes such as CTV (i.e., by transferring a high number of cells modified at a high transduction efficiency). Conclusions from this experiment are restricted to the validation of the functionality of the DivisionRecorder in dividing CD8$^+$ T cells. Splenic CD8$^+$ T cells were isolated using the Mouse CD8 T Lymphocyte Enrichment Set (BD Biosciences) and were subsequently stained with CellTrace™ Violet (Thermofisher). Next, cells were activated for 16h in T cell medium supplemented with 0.05 µg/mL SIINFEKL peptide and 60 IU/mL IL-2. Following this activation step, cells were seeded onto RetroNectin® (Takara Bio) coated plates and were transduced with DivisionRecorder virus by spinfection for 4h in the presence of IL-2 and SIINFEKL peptide. Analysis of CellTrace™ Violet signal by flow cytometry indicated that the cells had not undergone a full cell division post labeling. Subsequently, $6x10^6$ OT-I T cells were transferred into *Lm*-OVA infected recipients. Spleens were harvested 48h after adoptive transfer, processed into single cell suspensions and prepared for flow cytometric analysis. In order to accurately determine the fraction of DR^{RFP} cells per division during the initial stages of the proliferative burst when cumulative switching rate is still low, analysis of a large number of DivisionRecorder$^+$

OT-I T cells events is required. For this reason, a transduction efficiency of ~60% was chosen in these experiments, instead of the 10-15% transduction efficiency used in other experiments. Note that a high transduction efficiency will result in the more frequent occurrence of cells that carry multiple retroviral integrations. The presence of cells with multiple integrations will result in a higher, yet stable, DR^{RFP} acquisition rate, as compared to the experimental set-up used in the remainder of the study.

Ex vivo analysis of degranulation and cytokine secretion potential of memory T cells

Spleens were harvested from recipient mice at >60 days post-infection, and CD8 T cells were isolated using the Mouse CD8 T Lymphocyte Enrichment Set (BD Biosciences). Following isolation, T cells were plated at 10^6 cells per well in 96-well U bottom plates in T cell medium supplemented with 0.05 µg/mL SIINFEKL peptide to selectively activate OVA-specific T cells. Following a 4hr incubation, capacity of indicated T cell populations to either produce the indicated cytokines or to degranulate was assessed. To allow analysis of cytokine production, Brefeldin A (GolgiPlug™, BD Biosciences) was added 30 minutes after initiation of T cell stimulation. To allow analysis of degranulation, T cell medium was supplemented with anti-CD107a and anti-CD107b antibodies at the initiation of T cell stimulation, and Brefeldin A (GolgiPlug™, BD Biosciences) and Monensin (GolgiStop™, BD Biosciences) were added 30 minutes after initiation of T cell stimulation. At the end of the T cell stimulation period, cells were stained for KLRG1 and CD27 and prepared for flow cytometric analysis (see below).

Flow cytometric analysis

Cells were taken up in PBS (Invitrogen) supplemented with 0.5% bovine serum albumin (BSA, Fisher Scientific), and stained with antibodies directed against the indicated cell surface proteins (1:200 dilution), for 30min on ice. To allow detection of intracellular cytokine production, cells were fixed and permeabilized with CytoFix/CytoPerm™ (BD Biosciences) according to the manufacturer's protocol and subsequently stained using antibodies against IL-2, TNFα and IFNγ. To detect intranuclear Ki-67 expression, the Foxp3/Transcription factor Staining buffer set (eBioscience) was used. See **Supplementary Table 7** for list of antibodies used in the study. All samples were acquired on a BD LSR Fortessa™ (BD Bioscience); DR^{GFP} and DR^{RFP} cells were identified as CD8$^+$Vβ5$^+$CD45.2$^+$GFP$^+$tdTomato$^-$ and CD8$^+$Vβ5$^+$CD45.2$^+$GFP$^+$tdTomato$^+$, respectively. Flow cytometry data analysis was performed using FlowJo V10. An example of the used gating strategy is depicted in **Extended Data Fig. 10**.

For the moving average analysis depicted in **Fig. 3g** and **Extended Data Fig. 2e**, CD8$^+$Vβ5$^+$CD45.2$^+$GFP$^+$ events were exported and further processed using the R package FlowCore[50]. In brief, outlier events (i.e., antibody aggregates/cell doublets) were removed, fluorescence intensities of each of the cell surface proteins were normalized using an inverse hyperbolic sine transformation and subsequently scaled between 0 and 1. To

obtain the depicted moving averages, the fraction of DR^{RFP} cells was calculated within windows that each contained 10% of total cells, starting with the 10% of cells with the lowest expression levels for the indicated marker, and with subsequent windows moving up by steps of 2.5%.

Single cell RNA sequencing and data analysis of DivisionRecorder modified cells

The scRNAseq dataset of DivisionRecorder modified and unmodified OT-I memory T cells was obtained in two independent experiments, comprising 11 mice in total (See **Extended Data Fig. 3**). Experiment 1 included 3 mice containing DR^+ memory T cells (mouse 1-3), which were processed in a single batch. Experiment 2 included 4 mice containing DR^+ memory T cells (mouse 4-7) and 4 mice containing memory T cells derived from naïve OT-I T cells (unmodified, mouse 8-11), which were processed in two separate batches (batch 1: mouse 4-5 and mouse 8-9, batch 2: mouse 6-7 and mouse 10-11).

Spleens of DivisionRecorder$^+$ OT-I T cell recipient mice (n=7) or naïve OT-I T cell recipient mice (n=4) were harvested >65 days post-infection. Splenocytes were stained with fluorochrome-conjugated antibodies directed against CD8, CD45.2 and Vβ5 (See **Supplementary Table 7**), to allow purification of transferred cells by FACS using the BD FACSAria™ Fusion Flow Cytometer (BD Biosciences). DR^+ cells were subsequently FACS purified based on their expression of RFP and GFP. Following the isolation of DR^{GFP} and DR^{RFP} memory T cells by FACS (FACSAria Fusion, BD Biosciences), obtained cell populations were barcode-labeled with distinct anti-mouse TotalSeq™Hashtag antibodies (TotalSeq-A0301-0306, Biolegend), and pooled, with an equal number of cells from each mouse to form the total pool of cells for scRNA-sequencing. If the amount of sorted DR^{RFP} cells from a particular sample was limited, it was pooled together with another DR^{RFP} sample to reduce cell loss during cell hashing (as indicated in **Extended Data Fig. 3**). Single-cell RNA isolation and library preparation was performed according to the manufacturer's protocol of the 10X Genomics Chromium™ Single Cell 3' kit, and the cDNA library was sequenced on a NextSeq™ 550 Sequencing System (Illumina). Cumulative data tallied to a total of ~15,000 cells. Feature-barcode matrices were generated using the Cell Ranger software of the 10X Genomics Chromium™ pipeline. Cells that could be ascribed to multiple samples or to no sample (inferred from the detection of multiple or no Hash tags), cells with a transcript (UMI) count lower than 1,500 and cells with a mitochondrial-gene fraction higher than 0.12 were excluded from downstream analysis. Next, cells were further filtered based on gene counts, setting upper and lower thresholds separately for each sample-batch to control for differences in sequencing depth (gene-count-thresholds: Experiment 1 [1,200-3,000], experiment 2 batch 1 [800 -2,500], experiment 2 batch 2 [1,000-3,000]). Subsequent analysis of the remaining 11,767 cells was performed using the Seurat[51] and MetaCell[34] R packages.

To examine enrichment or depletion of DR^{RFP} cells within the different MetaCells, cell counts were first normalized across hashtags. Data obtained from the different mice were subsequently aggregated and used to calculate the ratio of DR^{RFP} versus DR^{GFP} cells in each MetaCell. The immune signature gene list used in several analyses was composed of gene clusters involved, or proposed to be involved in T cell function. The full gene list is described in **Supplementary Table 3**.

Differential gene-expression testing was performed using the FindMarkers function (Wilcoxon Rank Sum test) implemented in Seurat, comparing all ldT_{CM} to all hdT_{CM}. Significantly differentially expressed genes ($P < 0.05$) were subsequently used for gene-set enrichment analysis using the R package fgsea[52], testing for enriched gene-sets from the C7 immunologic or the H Hallmark gene-sets from Molecular Signatures Database (only including sets that consisted of >10 genes). Results from this analysis were filtered for collections deposited by Kaech and Goldrath (**Supplementary Table 2**), focusing on relevant CD8$^+$ T cell biology.

To calculate the QstemScore, the log2 enrichment values of genes that were positively or negatively associated with stem cell quiescence (**Supplementary Table 5**) were first summed within each MetaCell resulting in a positive and a negative score. QstemScore was then obtained by subtracting the negative-score from the positive-score.

Re-analysis of LCMV specific memory T cell scRNAseq dataset

Single cell transcriptomes from P14 memory T cells (harvested from spleen at day 90 post infection) were obtained from the Gene Expression Omnibus (accession GSE131847, sample GSM3822202). All single cells from this dataset were clustered applying the MetaCell algorithm. Next, T_{CM} MetaCells were determined based on the expression levels of core effector- and multipotency-related genes (**Supplementary Table 1**). QstemScores were then calculated for each of the T_{CM} MetaCells, and the 2 highest and 2 lowest scoring MetaCells were selected. Pearson correlations were subsequently calculated between each of these 4 T_{CM} MetaCells and all of the T_{CM} MetaCells from the OT-I dataset described here.

CTV-based serial transfer experiment and analysis

Spleens from OT-I and GFP;OT-I mice were harvested and CD8$^+$ T cells were isolated using the Mouse CD8 T Lymphocyte Enrichment Set (BD Biosciences) according to the manufacturer's protocol. The obtained cells were mixed in a 1:1 ratio and transferred to 4 primary recipient C57BL/6J-Ly5.1 mice ($1.5x10^6$ T cells per recipient), and 24 hours later recipients were infected with 5,000-10,000 CFU *Lm*-OVA. 30 days post-infection, spleens and lymph nodes were harvested and CD8$^+$ T cells were enriched using the Mouse CD8 T Lymphocyte Enrichment Set (BD Biosciences), replacing the supplied antibody-cocktail with a mixture of anti-mouse CD19, CD20 and CD4 biotinylated antibodies (used 1:200 each, See **Supplementary Table 7** for information on antibody clones). The enriched cell

pool was subsequently stained with CellTrace™ Violet (Thermofisher) and re-transferred into 4 infection-matched secondary C57BL/6J-Ly5.1 recipients. 74 days after secondary transfer (104 days post-infection) spleens and lymph nodes were harvested from the secondary recipients and stained with anti-mouse KLRG1-PE, CD27-APC, and CD45.2-AF700 (See **Supplementary Table 7** for information on antibody clones). Next, stained cell-pools were first enriched for transferred cells (i.e., CD45.2$^+$) through FACS using the BD FACSAria™ Fusion Flow Cytometer (BD Biosciences), and subsequently sorted again to obtain 4 populations of T_{CM} based on both GFP expression and CTV dilution: KLRG1$^-$CD27$^+$GFP$^+$Division0-2, KLRG1$^-$CD27$^+$GFP$^+$Division5+, KLRG1$^-$CD27$^+$GFP$^-$Division0-2, KLRG1$^-$CD27$^+$GFP$^-$Division5+. These cell pools were then further processed for tertiary transfer or single-cell RNA sequencing.

For tertiary transfer, GFP$^-$Division0-2 cells were mixed 1:1 with the GFP$^+$Division5+ cells (experiment 1), or GFP$^+$Division0-2 cells were mixed 1:1 with GFP$^-$Division5+ cells (experiment 2), thereby controlling for potential confounding effects of the donor strain. Next, 10,000 cells of either obtained cell pool were transferred in naive tertiary recipient C57BL/6J-Ly5.1 mice (3 mice for experiment 1, 4 mice for experiment 2). 24 hours later recipients were infected with 10,000 CFU *Lm*-OVA and the ratio of GFP$^+$ over GFP$^-$ cells within the transferred population (Ly5.2+) in blood was monitored by flow-cytometry over time.

For scRNAseq analysis, cell pools obtained by cell-sorting were barcode-labeled with distinct anti-mouse TotalSeq™ Hashtag antibodies (TotalSeq-A0301-0304, Biolegend), and subsequently pooled. Single-cell mRNA isolation and library preparation was performed according to the manufacturer's protocol of the 10X Genomics Chromium™ Single Cell 3' kit, and the cDNA library was sequenced on a NextSeq™ 550 Sequencing System (Illumina). Feature-barcode matrices were generated using the Cell Ranger software of the 10X Genomics Chromium™ pipeline, resulting in 13,064 single-cell transcriptomes. Cells that could be ascribed to multiple samples or to no sample (inferred from the detection of multiple or no Hashtags), cells with a transcript (UMI) count lower than 2,000 and cells with a mitochondrial-gene fraction higher than 0.12 were excluded from downstream analysis. Finally, cells with a gene-count of >2,800 were additionally excluded from further analysis. Subsequent analysis of the remaining 9,702 cells was performed using the Seurat[51] and MetaCell[34] R packages.

Differential gene-expression testing was performed using the FindMarkers function (Wilcoxon Rank Sum test) implemented in Seurat, comparing all CTV^{HI} (division0-2) cells to all CTV^{LO} (division5+) cells. Significantly differentially expressed genes ($P < 0.05$) were subsequently used for gene-set enrichment analysis using the R package fgsea[52], testing for enriched gene-sets from the C7 immunologic gene-sets (only including sets that consisted of >10 genes). Results from this analysis were filtered for collections

deposited by Kaech and Goldrath (**Supplementary Table 2**), focusing on relevant CD8$^+$ T cell biology.

For the MetaCell-based analysis, the number of cells within each hashtag-MetaCell combination was counted, and subsequently normalized to 1,000 cells within each hashtag. The ratios of CTV^{HI} over CTV^{LO} was then calculated separately for the GFP;OT-I and OT-I derived cells.

Statistical analysis

Flow cytometric data was acquired using BDFACSDiva (v8.0) software. Flow cytometric data was analyzed using Flowjo (v10.4.2), R (v6.3.1, 'Action of the Toes'), and FLowCore (v1.52.1). Single cell RNA sequencing data was analyzed using R (v 6.3.1), Seurat (v3.1.1), and MetaCell (v0.3.41). Data was visualized using Graphpad (V8.4.1, Prism software) and GGplot (v3.2.1). No statistical methods were used to pre-determine sample sizes, and sample sizes were chosen based on those reported in previous publications[13,53]. Data distribution was assumed to be normal but this was not formally tested. Mice were stratified according to age and sex where appropriate. Data collection and analysis were not performed blind to the conditions of the experiments. No data points were excluded from the analyses.

MATERIALS AND CORRESPONDENCE

Correspondence and material requests can be addressed to Ton N. Schumacher (t.schumacher@nki.nl) and Ferenc A. Scheeren (f.a.scheeren@lumc.nl). All commercially available reagents are listed in **Supplementary Table 8**.

Data availability

Transcriptomic data presented in the manuscript have been deposited to the Gene Expression Omnibus (GEO), and can be accessed under the GEO accessions GSE169154 and GSE184947. The gp33-specific P14 T cell scRNAseq dataset was retrieved from GEO (accession GSE131847, sample GSM3822202). All statistical source data of the figures presented in the present study are provided with this paper. Indicated gene sets used in gene set enrichment analyses were retrieved from the Molecular Signatures Database (MSigDB) at http://www.gsea-msigdb.org/gsea/msigdb. Any additional data supporting the findings of this study are available from the corresponding authors upon request.

Code availability

R scripts that were used to produce the main and extended data figures in the manuscript are available from GitHub (https://github.com/kasbress/DivisionRecorder_analysis).

REFERENCES

1. Hwang, L. N., Yu, Z., Palmer, D. C. & Restifo, N. P. The in vivo expansion rate of properly stimulated transferred CD8+ T cells exceeds that of an aggressively growing mouse tumor. *Cancer Res.* **66**, 1132–1138 (2006).
2. Yoon, H., Kim, T. S. & Braciale, T. J. The Cell Cycle Time of CD8+ T Cells Responding In Vivo Is Controlled by the Type of Antigenic Stimulus. *PLoS ONE* **5**, e15423 (2010).
3. Obar, J. J., Khanna, K. M. & Lefrançois, L. Endogenous Naive CD8+ T Cell Precursor Frequency Regulates Primary and Memory Responses to Infection. *Immunity* **28**, 859–869 (2008).
4. Blattman, J. N. *et al.* Estimating the precursor frequency of naive antigen-specific CD8 T cells. *J. Exp. Med.* **195**, 657–664 (2002).
5. Buchholz, V. R., Schumacher, T. N. M. & Busch, D. H. T Cell Fate at the Single-Cell Level. *Annu. Rev. Immunol.* **34**, 65–92 (2016).
6. Restifo, N. P. & Gattinoni, L. Lineage relationship of effector and memory T cells. *Curr. Opin. Immunol.* **25**, 556–563 (2013).
7. Akondy, R. S. *et al.* Origin and differentiation of human memory CD8 T cells after vaccination. *Nature* **552**, 362–367 (2017).
8. Sarkar, S. *et al.* Functional and genomic profiling of effector CD8 T cell subsets with distinct memory fates. *J. Exp. Med.* **205**, 625–640 (2008).
9. Obar, J. J. & Lefrançois, L. Early signals during CD8 T cell priming regulate the generation of central memory cells. *J. Immunol. Baltim. Md 1950* **185**, 263–272 (2010).
10. Kretschmer, L. *et al.* Differential expansion of T central memory precursor and effector subsets is regulated by division speed. *Nat. Commun.* **11**, 113 (2020).
11. Kinjyo, I. *et al.* Real-time tracking of cell cycle progression during CD8+ effector and memory T-cell differentiation. *Nat. Commun.* **6**, 6301 (2015).
12. Buchholz, V. R. *et al.* Disparate individual fates compose robust CD8+ T cell immunity. *Science* **340**, 630–635 (2013).
13. Gerlach, C. *et al.* Heterogeneous differentiation patterns of individual CD8+ T cells. *Science* **340**, 635–639 (2013).
14. Herndler-Brandstetter, D. *et al.* KLRG1+ Effector CD8+ T Cells Lose KLRG1, Differentiate into All Memory T Cell Lineages, and Convey Enhanced Protective Immunity. *Immunity* **48**, 716-729.e8 (2018).
15. Gerlach, C. *et al.* The Chemokine Receptor CX3CR1 Defines Three Antigen-Experienced CD8 T Cell Subsets with Distinct Roles in Immune Surveillance and Homeostasis. *Immunity* **45**, 1270–1284 (2016).
16. Reizel, Y. *et al.* Colon stem cell and crypt dynamics exposed by cell lineage reconstruction. *PLoS Genet.* **7**, e1002192 (2011).
17. Shlush, L. I. *et al.* Cell lineage analysis of acute leukemia relapse uncovers the role of replication-rate heterogeneity and microsatellite instability. *Blood* **120**, 603–612 (2012).
18. Kozar, S. *et al.* Continuous clonal labeling reveals small numbers of functional stem cells in intestinal crypts and adenomas. *Cell Stem Cell* **13**, 626–633 (2013).
19. Davis, F. M. *et al.* Single-cell lineage tracing in the mammary gland reveals stochastic clonal dispersion of stem/progenitor cell progeny. *Nat. Commun.* **7**, 13053 (2016).
20. Weber, T. S., Perié, L. & Duffy, K. R. Inferring average generation via division-linked labeling. *J. Math. Biol.* **73**, 491–523 (2016).
21. Tempany, J. C., Zhou, J. H., Hodgkin, P. D. & Bryant, V. L. Superior properties of CellTrace Yellow™ as a division tracking dye for human and murine lymphocytes. *Immunol. Cell Biol.* **96**, 149–159 (2018).

22. Lai, Y. The Relationship Between Microsatellite Slippage Mutation Rate and the Number of Repeat Units. *Mol. Biol. Evol.* **20**, 2123–2131 (2003).
23. Koole, W., Schäfer, H. S., Agami, R., van Haaften, G. & Tijsterman, M. A versatile microsatellite instability reporter system in human cells. *Nucleic Acids Res.* **41**, e158–e158 (2013).
24. Madisen, L. *et al.* A robust and high-throughput Cre reporting and characterization system for the whole mouse brain. *Nat. Neurosci.* **13**, 133–140 (2010).
25. Kallert, S. M. *et al.* Replicating viral vector platform exploits alarmin signals for potent CD8+ T cell-mediated tumour immunotherapy. *Nat. Commun.* **8**, 15327 (2017).
26. Wherry, E. J. *et al.* Lineage relationship and protective immunity of memory CD8 T cell subsets. *Nat. Immunol.* **4**, 225–234 (2003).
27. Becker, T. C. *et al.* Interleukin 15 Is Required for Proliferative Renewal of Virus-specific Memory CD8 T Cells. *J. Exp. Med.* **195**, 1541–1548 (2002).
28. Graef, P. *et al.* Serial transfer of single-cell-derived immunocompetence reveals stemness of CD8(+) central memory T cells. *Immunity* **41**, 116–126 (2014).
29. Olson, J. A., McDonald-Hyman, C., Jameson, S. C. & Hamilton, S. E. Effector-like CD8+ T Cells in the Memory Population Mediate Potent Protective Immunity. *Immunity* **38**, 1250–1260 (2013).
30. Youngblood, B. *et al.* Effector CD8 T cells dedifferentiate into long-lived memory cells. *Nature* **552**, 404–409 (2017).
31. Voehringer, D. *et al.* Viral infections induce abundant numbers of senescent CD8 T cells. *J. Immunol. Baltim. Md 1950* **167**, 4838–4843 (2001).
32. Lin, W.-H. W. *et al.* CD8 + T Lymphocyte Self-Renewal during Effector Cell Determination. *Cell Rep.* **17**, 1773–1782 (2016).
33. Johnnidis, J. B. *et al.* Inhibitory signaling sustains a distinct early memory CD8 ⁺ T cell precursor that is resistant to DNA damage. *Sci. Immunol.* **6**, eabe3702 (2021).
34. Baran, Y. *et al.* MetaCell: analysis of single-cell RNA-seq data using K-nn graph partitions. *Genome Biol.* **20**, 206 (2019).
35. Badovinac, V. P., Haring, J. S. & Harty, J. T. Initial T cell receptor transgenic cell precursor frequency dictates critical aspects of the CD8(+) T cell response to infection. *Immunity* **26**, 827–841 (2007).
36. Cheung, T. H. & Rando, T. A. Molecular regulation of stem cell quiescence. *Nat. Rev. Mol. Cell Biol.* **14**, 329–340 (2013).
37. Kurd, N. S. *et al.* Early precursors and molecular determinants of tissue-resident memory CD8 ⁺ T lymphocytes revealed by single-cell RNA sequencing. *Sci. Immunol.* **5**, eaaz6894 (2020).
38. Grassmann, S. *et al.* Early emergence of T central memory precursors programs clonal dominance during chronic viral infection. *Nat. Immunol.* **21**, 1563–1573 (2020).
39. Pais Ferreira, D. *et al.* Central memory CD8+ T cells derive from stem-like Tcf7hi effector cells in the absence of cytotoxic differentiation. *Immunity* **53**, 985-1000.e11 (2020).
40. Gattinoni, L. *et al.* Wnt signaling arrests effector T cell differentiation and generates CD8+ memory stem cells. *Nat. Med.* **15**, 808–813 (2009).
41. Gattinoni, L. *et al.* A human memory T cell subset with stem cell-like properties. *Nat. Med.* **17**, 1290–1297 (2011).
42. Laurenti, E. *et al.* CDK6 Levels Regulate Quiescence Exit in Human Hematopoietic Stem Cells. *Cell Stem Cell* **16**, 302–313 (2015).
43. Wilson, A. *et al.* Hematopoietic stem cells reversibly switch from dormancy to self-renewal during homeostasis and repair. *Cell* **135**, 1118–1129 (2008).

44. Schepers, A. G., Vries, R., van den Born, M., van de Wetering, M. & Clevers, H. Lgr5 intestinal stem cells have high telomerase activity and randomly segregate their chromosomes. *EMBO J.* **30**, 1104–1109 (2011).
45. Yan, K. S. *et al.* The intestinal stem cell markers Bmi1 and Lgr5 identify two functionally distinct populations. *Proc. Natl. Acad. Sci. U. S. A.* **109**, 466–471 (2012).
46. Clayton, E. *et al.* A single type of progenitor cell maintains normal epidermis. *Nature* **446**, 185–189 (2007).
47. Ito, M. *et al.* Stem cells in the hair follicle bulge contribute to wound repair but not to homeostasis of the epidermis. *Nat. Med.* **11**, 1351–1354 (2005).
48. An, Z. *et al.* A quiescent cell population replenishes mesenchymal stem cells to drive accelerated growth in mouse incisors. *Nat. Commun.* **9**, 378 (2018).
49. Sugimura, R. *et al.* Noncanonical Wnt Signaling Maintains Hematopoietic Stem Cells in the Niche. *Cell* **150**, 351–365 (2012).
50. Hahne, F. *et al.* flowCore: a Bioconductor package for high throughput flow cytometry. *BMC Bioinformatics* **10**, 106 (2009).
51. Butler, A., Hoffman, P., Smibert, P., Papalexi, E. & Satija, R. Integrating single-cell transcriptomic data across different conditions, technologies, and species. *Nat. Biotechnol.* **36**, 411–420 (2018).
52. Korotkevich, G. *et al. Fast gene set enrichment analysis*. http://biorxiv.org/lookup/doi/10.1101/060012 (2016) doi:10.1101/060012.
53. Kok, L. *et al.* A committed tissue-resident memory T cell precursor within the circulating CD8+ effector T cell pool. *J. Exp. Med.* **217**, e20191711 (2020).

EXTENDED DATA FIGURES

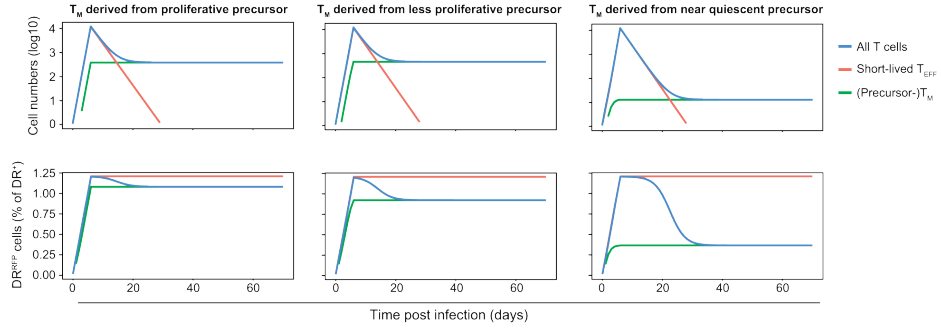

Extended Data Fig. 1. Simulation of different scenarios of memory T cell formation. Simulated data depicting a responding antigen-specific T cell population (blue), comprised of T_{EFF} undergoing clonal expansion and subsequent contraction (red), plus memory precursor T cells (MP, green) that develop into T_M. Activated T_{EFF} are modeled to divide rapidly for 6 days (expansion phase), die at a fixed rate throughout the response, and can differentiate into MP cells only during the expansion phase. Cell numbers (top row) and DR^{RFP} percentages (bottom row) are shown for 3 scenarios: (left) T_{EFF} can give rise to MP cells during the entire expansion phase, irrespective of the number of prior divisions, (middle) only T_{EFF} that have gone through at most 24 divisions can give rise to MP cells, or (right) only T_{EFF} that have gone through at most 10 divisions can give rise to MP cells. Note the strong decay in DR^{RFP} percentage that is observed during memory formation in case T cell memory is founded by T cells that have undergone few divisions. See **Supplementary Note 3** for detailed description and equations.

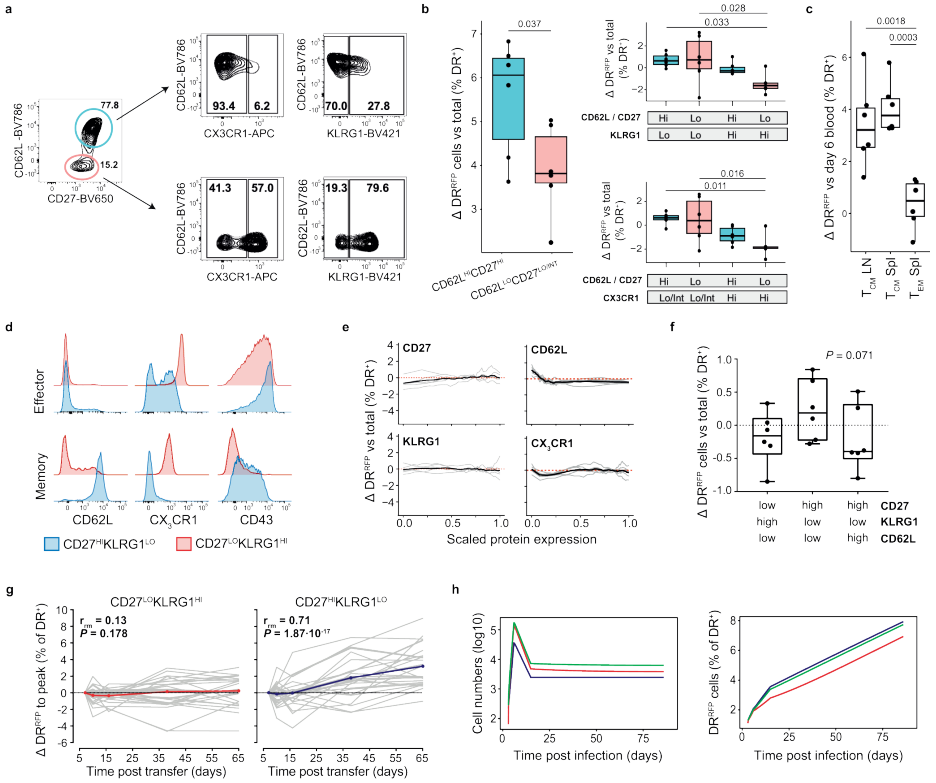

Extended Data Fig. 2. Evaluation of the division history of T cell subsets throughout a response to *Lm*-OVA. a, Gating strategy used to identify indicated T_M populations (d86) in spleen samples. **b,** DR^{RFP} percentages within splenic T_M populations (n=6 mice) as identified in panel a. **c,** DR^{RFP} percentages within the $CD27^{HI}KLRG1^{LO}$ T_{CM} subset in spleen and lymph nodes (LN) and within the $CD27^{LO}KLRG1^{HI}$ T_{EM} subset in spleen. **d,** Cell surface expression of CX_3CR1, CD62L, and CD43 within splenic $CD27^{LO}KLRG1^{HI}$ and $CD27^{HI}KLRG1^{LO}$ populations at the peak of the T_{EFF} phase (day 6 post infection) and in memory phase (day 86 post infection). **e,** Moving-average of surface marker expression of splenic DR^+ OT-I T cells during effector phase (day 6), depicted as in **Fig. 3g**. **f,** Boxplots depicting DR^{RFP} percentages within T_{EFF} (day 6 post infection) subsets in spleen (n=6 mice), relative to the total DR^{RFP} percentage. **g,** Kinetics of DR^{RFP} percentages within $CD27^{LO}KLRG1^{HI}$ (left) and $CD27^{HI}KLRG1^{LO}$ (right) DR^+ OT-I T cell populations in blood. Values are relative to the percentage of DR^{RFP} cells detected at the peak of the response (day 6). Grey lines represent individual mice (n = 22), red and blue lines indicate group mean. **h,** Simulation of the phenotype model (See **Supplementary Note 5** for details) illustrating a scenario in which conversion of $CD27^{HI}KLRG1^{LO}$ to $CD27^{LO}KLRG1^{HI}$ cells occur only after the peak of the response at a low rate. Depicted are the overall cell numbers (left), and the percentage DR^{RFP} cells of DR^+ OT-I T cells (right) in $CD27^{HI}KLRG1^{LO}$ cells (blue), $CD27^{LO}KLRG1^{HI}$ cells (red) and the total T cell population (green). Note that in this scenario the fraction DR^{RFP} within the terminally differentiated $CD27^{LO}KLRG1^{HI}$ population would increase to almost twice the experimentally observed frequency. All depicted data are representative of at least two independent experiments. Boxplots (**c, d, g**) represent group median and $25^{th}/75^{th}$ percentiles, whiskers indicate the interquartile range multiplied by 1.5 (**c, d**) or min/max (**g**), dots indicate individual samples. *P* values were determined by one-way ANOVA followed by Tukey's HSD post-hoc test (**c** and **d**), two-sided Student's T test (**c**), two-sided repeated measurement correlation test (**h**), or two-sided Friedman test (**g**). All significant (< 0.05) P values are indicated in the plots.

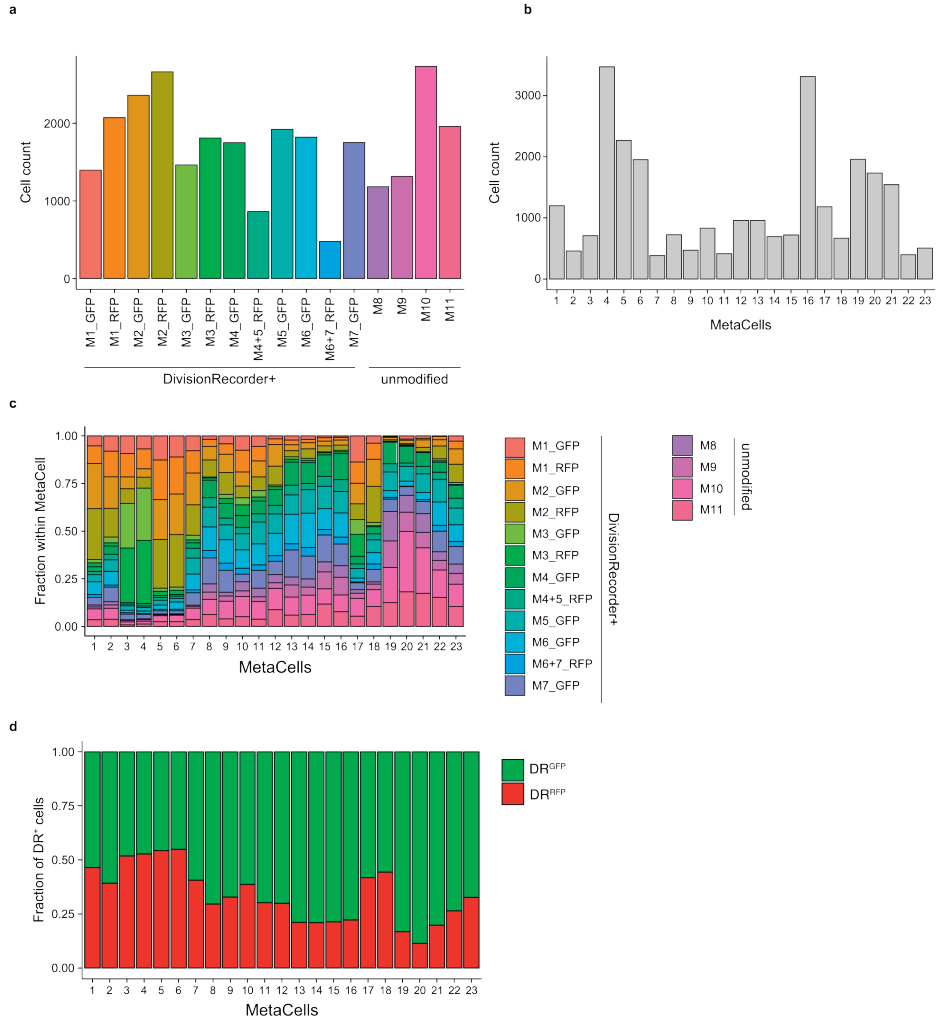

Extended Data Fig. 3. Single cell mRNA sequencing of DivisionRecorder⁺ and unmodified memory T cells. Single cell mRNA sequencing was performed on DivisionRecorder modified and unmodified OT-I memory T cells (Day 75 and 85 post *Lm*-OVA infection), isolated from spleens (n=7 mice with DR+ memory T cells; n=4 with unmodified memory T cells). Obtained data were aggregated from two independent experiments (Experiment 1: M1-3; Experiment 2: M4-11). All cells were jointly analysed and clustered. **a,** Cell count per sample. **b,** Total cell count per MC. **c,** Sample composition of each MC. **d,** Relative contribution of DR^{GFP} and DR^{RFP} to the total DR^+ pool within each MC.

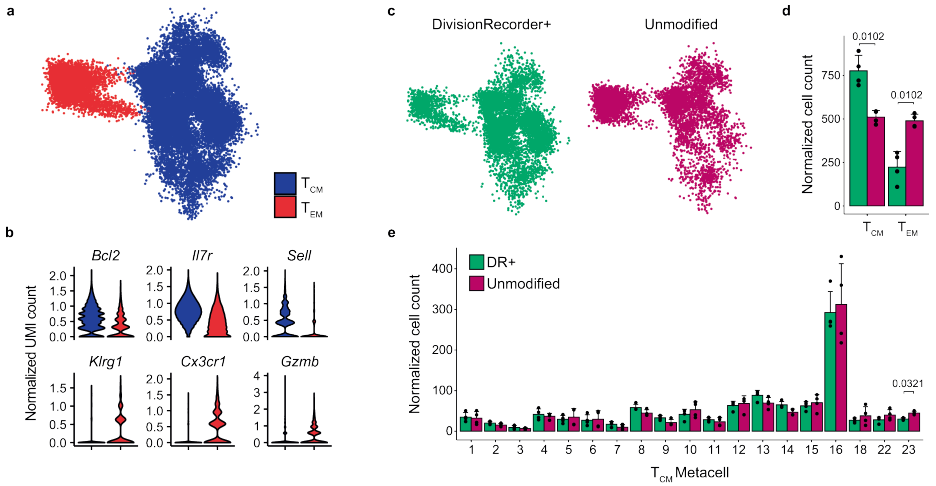

Extended Data Fig. 4. T_{CM} transcriptional states are preserved in DR$^+$ OT-I T cells. Comparison of transcriptional states of splenic memory T cells generated by either DivisionRecorder modified, or unmodified OT-I T cells (Day 75 and 85 post *Lm*-OVA infection). **a-b,** Memory OT-I T cells cluster into T_{CM} (blue) and T_{EM} (red). 2D projection colored by subset (**a**), and violin plots depicting normalized UMI counts of selected genes (**b**) are shown. **c,** 2D projection of either DR$^+$ (left) or unmodified (right) memory OT-I T cells. **d,** Contribution of DR$^+$ and unmodified memory T cells to the T_{CM} and T_{EM} subsets. **e,** Contribution of DR$^+$ and unmodified OT-I T cells to the 19 MCs that jointly make up the T_{CM} subset. Dots indicate individual mice (n=3 per condition). Note that all T_{CM} states are generated in near-equal proportions by DR$^+$ and unmodified memory T cells. Depicted scRNAseq data was obtained from 6 individual mice, and was aggregated from 2 independent experiments. *P* values were determined by two-sided Student's T test followed by Bonferroni correction for multiple testing (**d** and **e**). *P* values < 0.05 are indicated.

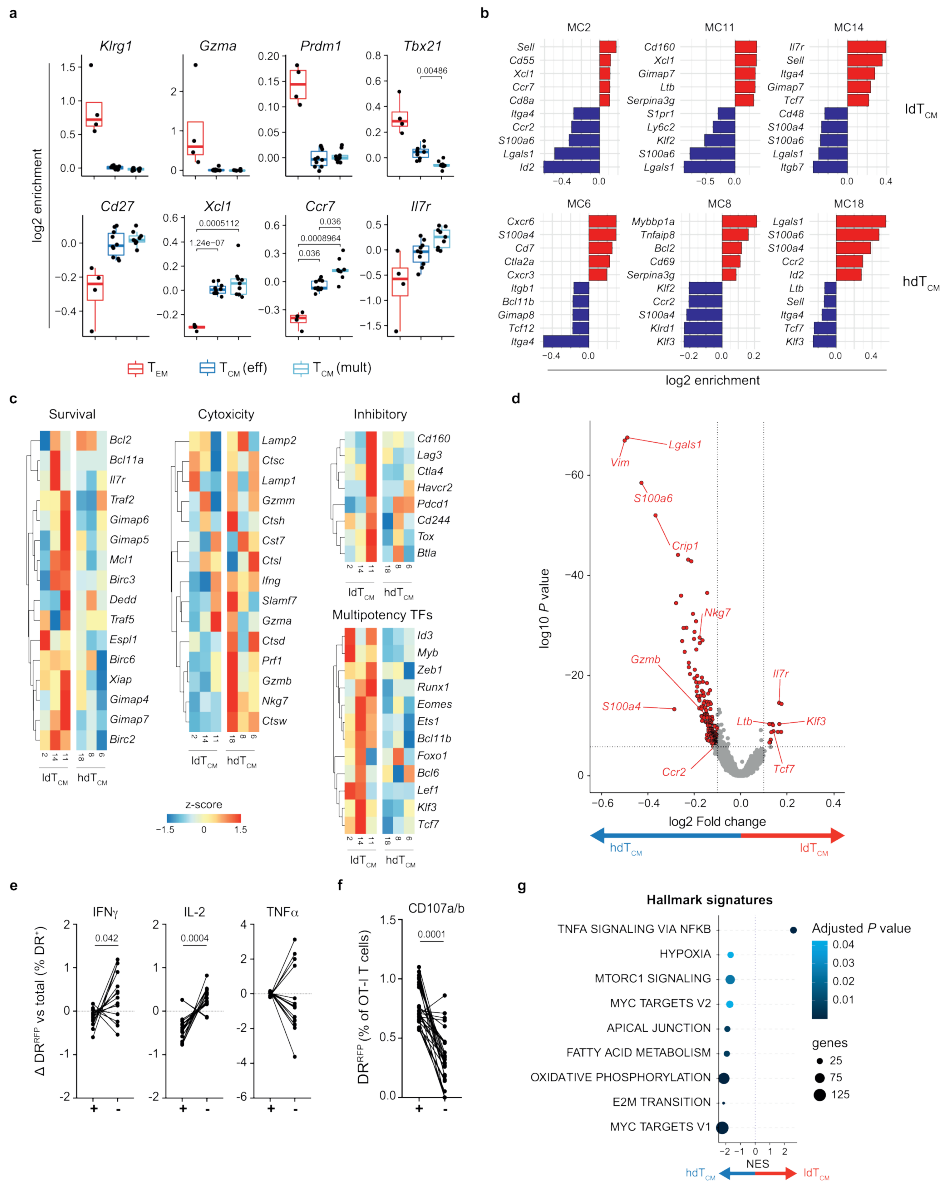

Extended Data Fig. 5. Replicative history identifies distinct transcriptional states within the T_{CM} pool. Single cell transcriptomic profiling of DR$^+$ T cells obtained from spleen in memory phase (Day 75 and 85 post *Lm*-OVA infection). **a,** Log2 enrichment of selected genes in each MC cluster. Boxplots indicate group median and 25th/75th percentiles, whiskers indicate the interquartile range multiplied by 1.5, dots signify individual MCs. The phenotype clusters T_{EM}, T_{CM}(eff) and T_{CM}(mult) contain 4, 9 and 10 MCs, respectively. For definition of T_{CM}(eff) and T_{CM}(mult), see Fig. 4B. **b,** Top and bottom marker genes of ldT_{CM} (Top, MC2, 11, 14) and hdT_{CM} (Bottom, MC6, 8, 18), see Fig. 4D for ldT_{CM} and hdT_{CM} definitions. **c,** Heatmaps depicting z-score transformed enrichment values of genes related to cell survival (left), cytotoxicity and effector function (middle), inhibitory markers (top-right), and transcription factors involved in T cell multipotency

(bottom-right). Expression is depicted for the 3 ldT_{CM} and 3 hdT_{CM} MCs. **d,** Volcano plot depicting differentially expressed genes in ldT_{CM} versus hdT_{CM}. Significantly (adjusted P-value < 0.05) differentially expressed genes are depicted in red. Selected genes are highlighted. **e,** Cytokine release of $CD27^{HI}KLRG1^{LO}$ DR^{+} T cells (isolated from spleen at day >60 post infection) 4 hours post *ex vivo* stimulation. Percentage DR^{RFP} cells within cytokine producers (+) and non-producers (-), relative to the average DR^{RFP} percentage within each sample, is depicted. Lines connect individual *ex vivo* stimulated samples samples (n=12), obtained from 3 mice. **f,** *Ex vivo* degranulation of $CD27^{HI}KLRG1^{LO}$ DR^{+} T cells (isolated from spleen at day >60 post infection) 4 hours post *ex vivo* stimulation. Percentage DR^{RFP} cells within the CD107a/b positive (+) or negative (-) cell populations is depicted. Lines connect individual samples *ex vivo* stimulated samples (n=17), obtained from 5 mice. **g,** Enrichment of gene signatures from MSigDB (Hallmark) by gene set enrichment analysis comparing ldT_{CM} and hdT_{CM}. Data depicted was accumulated in two independent experiments (3-4 mice per experiment). *P* values were determined by Tukey's HSD test (**a**), Wilcoxon Rank Sum test with Bonferroni correction (**d**), two-sided Wilcoxon signed-rank test (**e, f**), the FGSEA algorithm followed by the Benjamini-Hochberg procedure (**g**). *P* values < 0.05 are indicated.

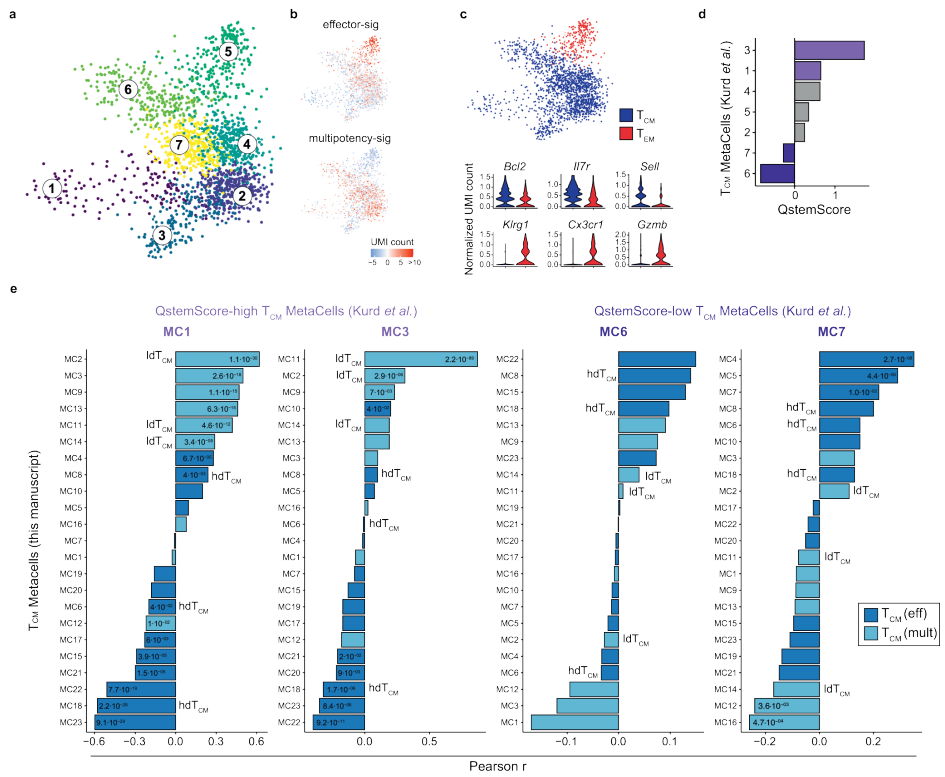

Extended Data Fig. 6. gp33-specific P14 T_{CM} with increased expression of genes associated with replicative quiescence resemble OT-I ldT_{CM}. Re-analysis of scRNAseq profiled splenic of P14 memory T cells, published in Kurd *et al.* (*Kurd et al., Science Immunology, 2020*). **a-b,** 2D projection of P14 memory T cells 90 days post LCMV infection, colors indicate individual MCs (**a**), or the relative expression of effector- and multipotency-associated genes (**b**). Gene list in **Supplementary Table 1**. **c,** P14 memory T cells cluster into T_{CM} (blue) and T_{EM} (red). 2D projection colored by subset (top), and violin plots depicting normalized UMI counts of selected genes (bottom) are shown. **d,** QstemScore of all T_{CM} MCs in the Kurd *et al.* dataset. **e,** Pearson correlations between the Kurd et al. P14 T_{CM} MCs that score high (MC1, 3) or low (MC6, 7) for QstemScore, and all OT-I T_{CM} MCs described here. Data are depicted as waterfall plots, asterisks indicate significant correlations. T_{CM}(eff), T_{CM}(mult), ldT_{CM} and hdT_{CM} MCs are defined in **Figure. 4**. *P* values were determined by two-sided Pearson correlation test followed by Bonferroni correction (**e**). *P* values < 0.05 are indicated in the plots.

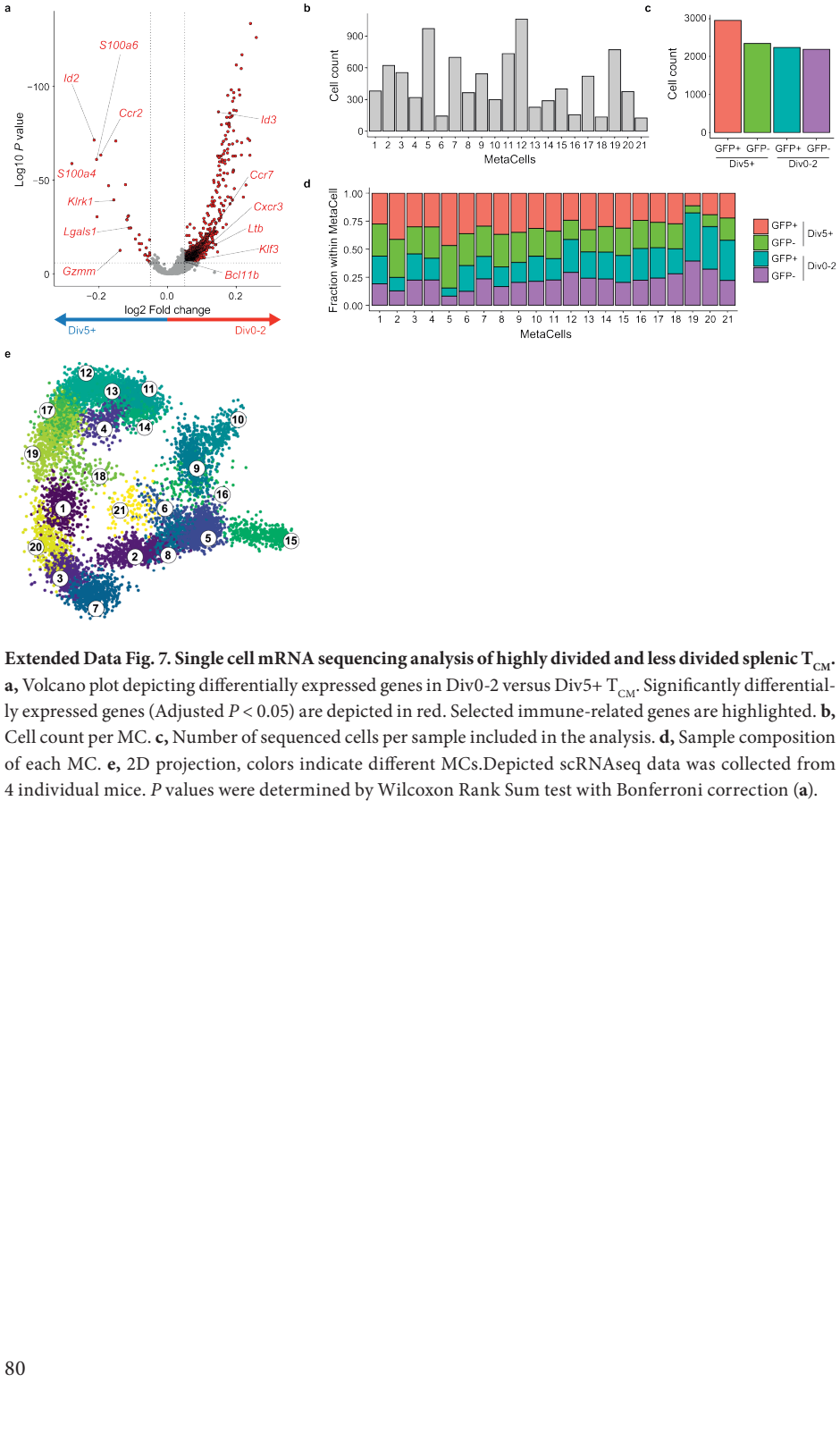

Extended Data Fig. 7. Single cell mRNA sequencing analysis of highly divided and less divided splenic T_{CM}. **a,** Volcano plot depicting differentially expressed genes in Div0-2 versus Div5+ T_{CM}. Significantly differentially expressed genes (Adjusted $P < 0.05$) are depicted in red. Selected immune-related genes are highlighted. **b,** Cell count per MC. **c,** Number of sequenced cells per sample included in the analysis. **d,** Sample composition of each MC. **e,** 2D projection, colors indicate different MCs.Depicted scRNAseq data was collected from 4 individual mice. *P* values were determined by Wilcoxon Rank Sum test with Bonferroni correction (**a**).

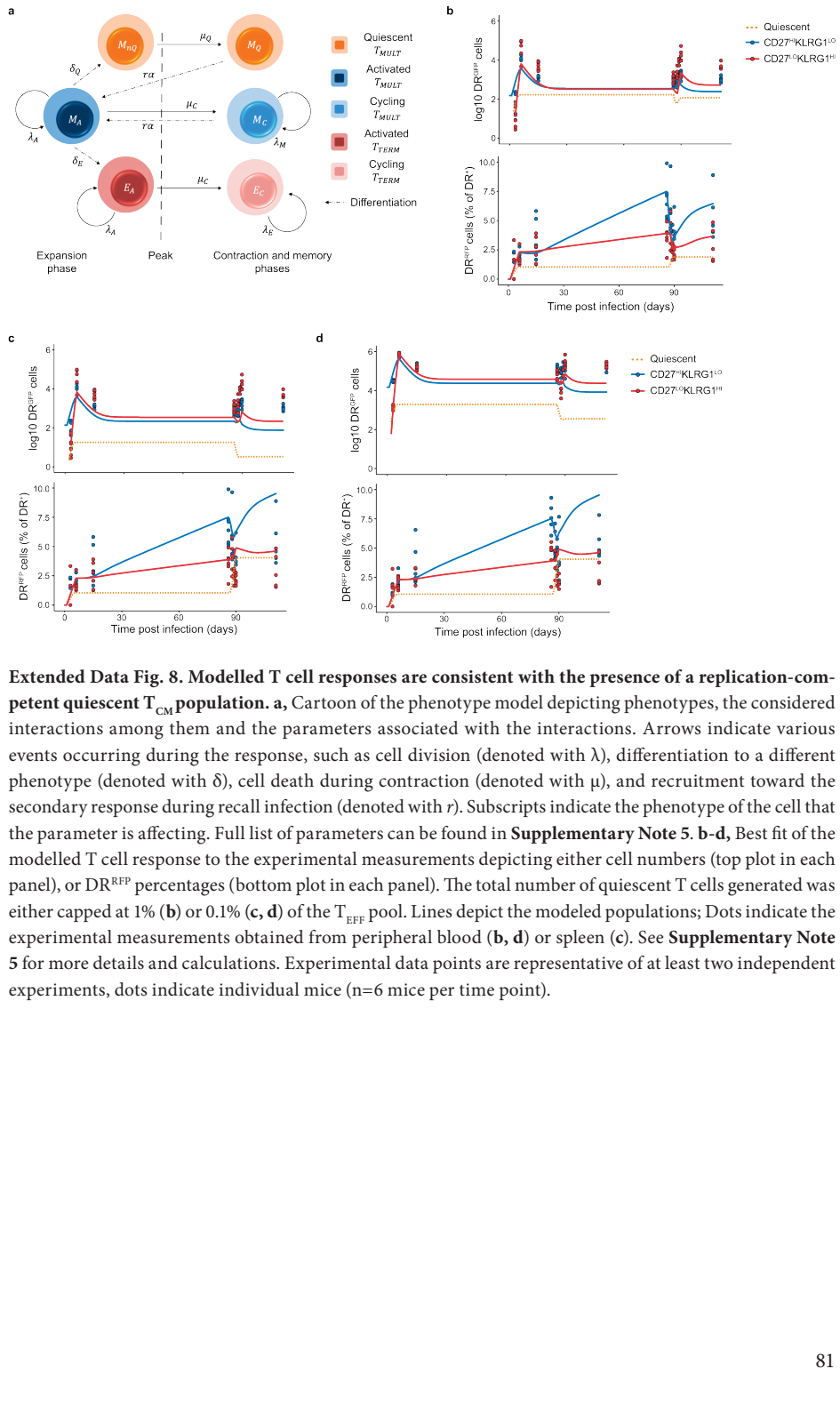

Extended Data Fig. 8. Modelled T cell responses are consistent with the presence of a replication-competent quiescent T_{CM} population. a, Cartoon of the phenotype model depicting phenotypes, the considered interactions among them and the parameters associated with the interactions. Arrows indicate various events occurring during the response, such as cell division (denoted with λ), differentiation to a different phenotype (denoted with δ), cell death during contraction (denoted with μ), and recruitment toward the secondary response during recall infection (denoted with *r*). Subscripts indicate the phenotype of the cell that the parameter is affecting. Full list of parameters can be found in **Supplementary Note 5**. **b-d,** Best fit of the modelled T cell response to the experimental measurements depicting either cell numbers (top plot in each panel), or DR^{RFP} percentages (bottom plot in each panel). The total number of quiescent T cells generated was either capped at 1% (**b**) or 0.1% (**c, d**) of the T_{EFF} pool. Lines depict the modeled populations; Dots indicate the experimental measurements obtained from peripheral blood (**b, d**) or spleen (**c**). See **Supplementary Note 5** for more details and calculations. Experimental data points are representative of at least two independent experiments, dots indicate individual mice (n=6 mice per time point).

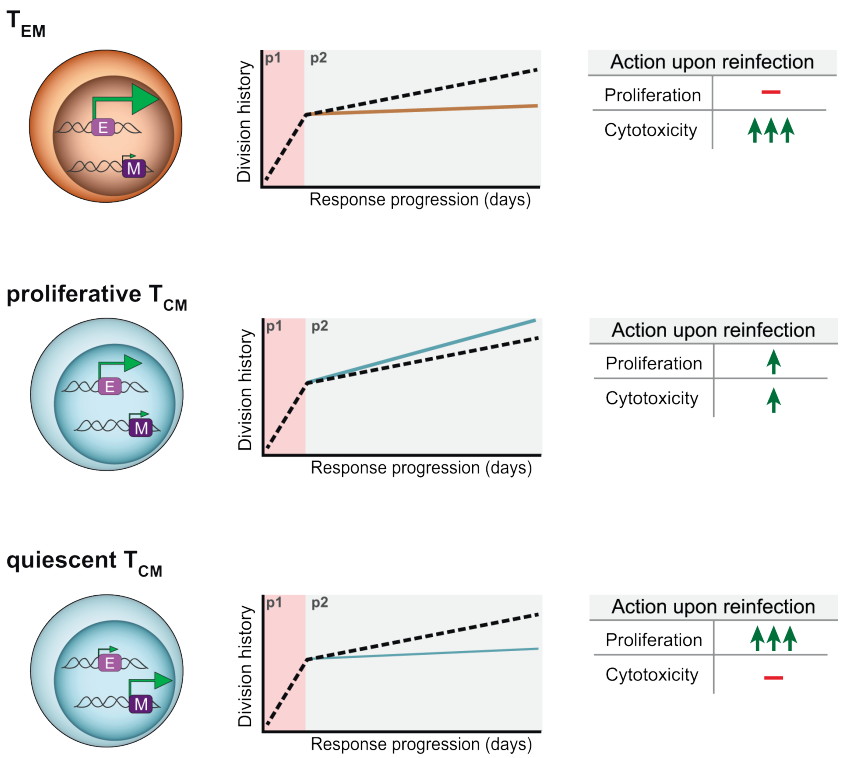

Extended Data Fig. 9. Model describing replicative behaviors in the CD8⁺ memory T cell pool. Upon infection, antigen-specific CD8⁺ T cells activate and rapidly expand (phase 1, p1). Following pathogen clearance (p2), a subset of memory T cells continues to divide, resulting in a progressive increase in the replicative history of the overall T cell memory pool (dotted line). Within this population, three separate behaviors of transcriptionally disparate memory T cell pools can be distinguished.
Top) Terminally differentiated T_{EM} cells that cease division after the inflammation phase (p1) and that are marked by high transcription of effector- and minimal expression of multipotency-associated genes ([E], [M]). Upon reactivation, these cells exert rapid effector functions, but lack the potential to re-expand.
Middle) A subgroup of T_{CM} that continues to proliferate in the memory phase, exhibits diminished levels of multipotency-associated transcripts, and that abundantly expresses effector-associated genes. Although the functionality of these cells upon reinfection requires further study, their heightened expression of effector-associated genes suggests that these cells exert cytotoxic activity upon reinfection. The contribution of these cells to the secondary T_{EFF} pool is limited.
Bottom) A subgroup of T_{CM} cells that shows low expression of effector-associated genes but increased expression of multipotency-associated genes, and that exists in a near-quiescent state after the inflammation phase. Upon renewed infection, this cell pool is primarily responsible for the generation of a new wave of secondary T_{EFF}. Based on their transcriptional profile, these cells are expected to have limited immediate cytotoxic functions.

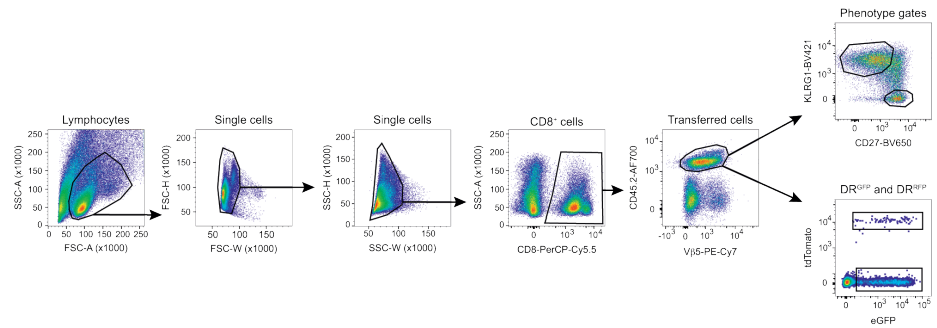

Extended Data Fig. 10. Gating strategy. General gating applied to flow cytometry data presented in the study. Single lymphocytes were first selected using morphology gates, and were subsequently gated on CD8⁺ T cells and transferred OT-I T cells (Vb5⁺CD45.2⁺). Next, DR^{RFP} and RF^{GFP} could be directly selected, or first separated by phenotype depending on the analysis. The data presented here was analyzed from blood of a recipient of DR⁺ cells, and was acquired 6 days post infection with *Lm*-OVA. Phenotype gates other than those shown here are defined in their respective figures.

SUPPLEMENTARY TABLES

Effector-sig	Multipotency-sig
Id2	*Myb*
Ifng	*Tcf7*
Tbx21	*Bach2*
Lgals1	*Eomes*
Gzmb	*Sell*
Prf1	*Ccr7*
Prdm1	*Il7r*
Klrg1	*Bcl2*
Cx3cr1	

Supplementary Table 1. Manually curated effector-associated and multipotency-associated gene signatures. Listed in order of appearance (top-to-bottom) in the heatmap depicted in **Figure 4b**.

gs_name	gs_id	gs_pmid	gs_exact_source	gs_description
GOLDRATH_EFF_VS_MEMORY_CD8_TCELL_DN	M3044	16492737	GSE1000002_1582_200_DN	Genes down-regulated in comparison of effector CD8 T cells relative to memory CD8 T cells.
GOLDRATH_EFF_VS_MEMORY_CD8_TCELL_UP	M3041	16492737	GSE1000002_1582_200_UP	Genes up-regulated in effector CD8 T cells relative to memory CD8 T cells.
GOLDRATH_NAIVE_VS_EFF_CD8_TCELL_DN	M3036	16492737	GSE1000002_1580_200_DN	Genes down-regulated in naive CD8 T cells relative to effector CD8 T cells.
GOLDRATH_NAIVE_VS_EFF_CD8_TCELL_UP	M3035	16492737	GSE1000002_1580_200_UP	Genes up-regulated in naive CD8 T cells relative to effector CD8 T cells.
GOLDRATH_NAIVE_VS_MEMORY_CD8_TCELL_DN	M3039	16492737	GSE1000002_1581_200_DN	Genes down-regulated in naive CD8 T cells relative to memory CD8 T cells.
GOLDRATH_NAIVE_VS_MEMORY_CD8_TCELL_UP	M3038	16492737	GSE1000002_1581_200_UP	Genes up-regulated in naive CD8 T cells relative to memory CD8 T cells.
KAECH_DAY15_EFF_VS_MEMORY_CD8_TCELL_DN	M3032	12526810	GSE1000001_1579_200_DN	Genes down-regulated in effector CD8 T cells at contraction phase (day 15 after LCMV-Armstrong infection) relative to memory CD8 T cells (day 40+ after LCMV-Armstrong infection).
KAECH_DAY15_EFF_VS_MEMORY_CD8_TCELL_UP	M3030	12526810	GSE1000001_1579_200_UP	Genes up-regulated in effector CD8 T cells at contraction phase (day 15 after LCMV-Armstrong infection) relative to memory CD8 T cells (day 40+ after LCMV-Armstrong infection).
KAECH_DAY8_EFF_VS_DAY15_EFF_CD8_TCELL_DN	M3025	12526810	GSE1000001_1577_200_DN	Genes down-regulated in effector CD8 T cells at the peak expansion phase (day 8 after LCMV-Armstrong infection) relative to effector CD8 T cells at contraction phase (day 15 after LCMV-Armstrong infection).

Supplementary Table 1. Continued.

gs_name	gs_id	gs_pmid	gs_exact_source	gs_description
KAECH_DAY8_EFF_VS_DAY15_EFF_CD8_TCELL_UP	M3023	12526810	GSE1000001_1577_200_UP	Genes up-regulated in effector CD8 T cells at the peak expansion phase (day 8 after LCMV-Armstrong infection) relative to effector CD8 T cells at contraction phase (day 15 after LCMV-Armstrong infection).
KAECH_DAY8_EFF_VS_MEMORY_CD8_TCELL_DN	M3028	12526810	GSE1000001_1578_200_DN	Genes down-regulated in effector CD8 T cells at the peak expansion phase (day 8 after LCMV-Armstrong infection) relative to memory CD8 T cells (day 40+ after LCMV-Armstrong infection).
KAECH_DAY8_EFF_VS_MEMORY_CD8_TCELL_UP	M3027	12526810	GSE1000001_1578_200_UP	Genes up-regulated in effector CD8 T cells at the peak expansion phase (day 8 after LCMV-Armstrong infection) relative to memory CD8 T cells (day 40+ after LCMV-Armstrong infection).
KAECH_NAIVE_VS_DAY15_EFF_CD8_TCELL_DN	M3017	12526810	GSE1000001_1575_200_DN	Genes down-regulated in naive CD8 T cells relative to effector CD8 T cells at contraction phase (day 15 after LCMV-Armstrong infection).
KAECH_NAIVE_VS_DAY15_EFF_CD8_TCELL_UP	M3014	12526810	GSE1000001_1575_200_UP	Genes up-regulated in naive CD8 T cells relative to effector CD8 T cells at contraction phase (day 15 after LCMV-Armstrong infection).
KAECH_NAIVE_VS_DAY8_EFF_CD8_TCELL_DN	M3013	12526810	GSE1000001_1574_200_DN	Genes down-regulated in naive CD8 T cells relative to effector CD8 T cells at the peak expansion phase (day 8 after LCMV-Armstrong infection).
KAECH_NAIVE_VS_DAY8_EFF_CD8_TCELL_UP	M3012	12526810	GSE1000001_1574_200_UP	Genes up-regulated in naive CD8 T cells relative to effector CD8 T cells at the peak expansion phase (day 8 after LCMV-Armstrong infection).

Supplementary Table 1. Continued.

gs_name	gs_id	gs_pmid	gs_exact_source	gs_description
KAECH_NAIVE_VS_MEMORY_CD8_TCELL_DN	M3022	12526810	GSE1000001_1576_200_DN	Genes down-regulated in naive CD8 T cells relative to memory CD8 T cells (day 40+ after LCMV-Armstrong infection).
KAECH_NAIVE_VS_MEMORY_CD8_TCELL_UP	M3020	12526810	GSE1000001_1576_200_UP	Genes up-regulated in naive CD8 T cells relative to memory CD8 T cells (day 40+ after LCMV-Armstrong infection).

Supplementary Table 2. Gene-sets used from the MSigDB collection C7

Ly96	Cd38	Tlr3	Itga5	Fbxo10	Tgfbr2	Prdm2
Il1rl2	Tlr1	Il12rb1	Il1rap	Tgfbr1	Cx3cr1	Prdm16
Il1rl1	Tlr6	Jak3	Itgb5	Nr4a3	Clec3b	Klf3
Il18r1	Il12rb2	Il15	Cd86	Fbxo42	Fbxo48	Ezh2
Il18rap	Cd8b1	Il27ra	Cd80	Fbxo6	Bcl11a	Prdm5
Cd28	Cd8a	Itgb1	Cd200r1	Fbxo44	Havcr2	Tcf7l1
Cxcr4	Il17ra	Il3ra	Cd200r4	Tgfbr3	Serpinf2	Foxp1
Cd55	Klrg1	Il17rd	Cd200	Fbxo21	Traf4	Sox5
Tnfsf4	Cd163	Il17rb	Cd96	P2rx7	Lgals9	Klf13
Sell	Cd4	Tox4	Cd47	P2rx4	Fbxo47	Myb
Xcl1	Cd27	Ltb4r1	Il10rb	Bcl7a	Lgals8	Foxo3
Cd247	Tnfrsf1a	Gzmc	Ifngr2	Bcl7b	Serpinb1a	Prdm1
Cd244	Cd9	Gzmb	Tnfrsf12a	Fbxo24	Serpinb6b	Icosl
Ly9	Klrb1c	Tnfrsf10b	Cd320	Kdelr2	Serpinb9	Tcf3
Cd48	Klrb1f	Cxcr5	Ly6g5b	Gimap8	Serpinb6a	Klf16
Cd84	Cd69	Cd3g	Ltb	Gimap9	Prr7	Prdm4
Cd46	Klre1	Cd3d	Tnf	Gimap4	Tgfbi	Socs2
Il2ra	Klrd1	Cd3e	Cd2ap	Gimap6	Ctla2b	Stat6
Il15ra	Klrk1	Il10ra	Tnfrsf21	Gimap7	Ctla2a	Stat2
Cd302	Klrc3	Il18	Tnfaip8l1	Gimap1	Fbxo33	Jund
Ly75	Klrc2	Il20rb	Tnfsf9	Gimap5	Serpina12	Klf2
Itga6	Klrc1	Ccr9	Tnfsf14	Gimap3	Serpina3f	Junb
Itga4	Klri2	Cxcr6	Tnfaip8	Bcl2l13	Serpina3g	Tcf25
Itgav	Klra4	Ccr3	Cd74	Clec4a1	Bcl11b	Socs4
Cd82	Klra8	Ccr2	Cd226	Clec4a3	Traf3	Klf12
Cd44	Klra9	Ccr5	Cd5	Clec4a2	Fbxo4	Dnmt1
Il1b	Klra7	Tnfrsf13b	Cd6	Clec4n	Fbxo32	Prdm10
Cd93	Klra3	Cd68	Jak2	Lag3	Lgals1	Tcf12
Cd40lg	Klra2	Tnfsf13os	Cd274	Clec2i	Nr4a1	Eomes
Cd99l2	Cd3eap	Itgae	Tgfbrap1	Clec2g	Clec16a	Tcf7
Il2rg	Cd79a	Tnfaip1	Ctla4	Clec2d	Bcl6	Mybbp1a
Itgb1bp2	Ltbp4	Itga3	Serpine2	Clec12a	Fbxo45	Tbx21
Cxcr3	Cd22	Ccr7	Fbxo36	Bcl2l14	Fbxo40	Socs7
Tlr7	Il4i1	Ccr10	Pdcd1	Fbxo46	Traf7	Stat3
Il7	Cd37	Itga2b	Bcl2	Bcl3	Fbxo11	Socs3
Tnfsf10	Il16	Itgb3	Serpinc1	Tgfb1	Fbxo38	Klf6

Il2	Il18bp	Cd79b	Fasl	Fbxo27	Pdcd1lg2	Sox4
Tlr2	Il4ra	Cd300a	Fbxo28	Fbxo17	Fas	Klf11
Cd1d1	Il21r	Cd300c2	Tgfb2	Lgals4	Pdcd11	Id2
Cd5l	Cd19	Cd300lf	Traf5	Clec11a	Mybl1	Klf10
Il6ra	Cd2bp2	Itgb4	Fbxo18	Bcl2l12	Stat4	Tcf20
Tnfaip8l2	Itgal	Cd7	Traf2	Kdelr1	Stat1	Socs1
Itga10	Itgam	Ly86	Traf1	Lat	Icos	Runx1
Cd160	Itgax	Cd83	Nr4a2	Bcl7c	Klf7	Prdm15
Cd101	Itgad	Cd180	Traf6	Tgfb1i1	Gata3	Prdm9
Cd2	Cd163l1	Il6st	Fbxo3	Fbxo5	Zeb2	Tcf19
Cd53	Cd151	Gzma	Bcl2l11	Fbxo30	Zeb2os	Runx2
Tox	Cd81	Gzmk	Bcl2l1	Fbxo7	Prdm11	Runx2os2
Il11ra1	Tnfrsf26	Itga2	Pdcd10	Tgfbr3l	Sox12	Runx2os1
Cd72	Tnfrsf22	Itga1	Serpini1	Fbxo25	Id1	Foxp4
Tnfsf8	Tnfrsf23	Itgb1bp1	S100a1	Fbxo8	Mybl2	Socs5
Tlr4	Tnfaip3	Il7r	S100a13	Fbxo31	Foxp3	Zeb1
Itgb3bp	Ifngr1	Ly6d	S100a3	Lgals3	Foxo4	Gata6
Jak1	Cd164	Ly6k	S100a2	Fbxo34	Klf8	Tcf4
Tlr12	Cd24a	Ly6e	S100a4	Bcl2l2	Foxo1	Socs6
Cd52	Prf1	Ly6i	S100a5	Bcl9l	Bach2	Klf9
Tnfrsf1b	Itgb2	Ly6a	S100a6	Fbxo22	Bach2os	Tcf7l2
Tnfrsf9	Gzmm	Ly6c1	S100a11	Fbxo9	Klf4	S1pr1
Tnfrsf25	Ifng	Ly6c2	S100a10	Bcl2a1d	Jun	Jakmip1
Tnfrsf14	Ifngas1	Il2rb	Bcl9	Bcl2a1a	Junos	S1pr4
Tnfrsf4	Cd63	Tnfrsf13c	Bcl2l15	Bcl2a1b	Runx3	S1pr2
Tnfrsf18	Tnfsf13b	Itgb7	Bcl10	Bcl2a1c	Id3	S1pr5

Supplementary Table 3. Full list of immune-associated genes used in scRNAseq data analysis.

Up in ldT_{CM}	Up in hdT_{CM}
Il7r	Ccr2
Stat4	S100a11
Tcf7	Tbx21
Klf3	Klrc1
Foxp1	Il2rb
Sell	Jund
Itga4	Cd52
Cd84	Cd48
Eomes	Gzmb
Ltb	Prf1
Gimap6	Pdcd10
Cd28	Itgb7
Serpina3g	Cd2
Xcl1	Cd3g
Gzmk	S100a10
Gimap7	S100a4
Stat1	Cd8b1
	Lgal1
	S100a13
	S100a6
	Klrk1
	Ly6c2
	Klf2

Supplementary Table 4. Full gene lists from heatmap depicted in Figure 4G in order of appearance (left-to-right)

Positive association		Negative Association	
Ccnd3	*Phf1*	*Anln*	*Birc5*
Pdk1	*Ctdsp1*	*Ccna2*	*Ccnb1*
Smarca2	*Thrashings*	*Ccne2*	*Ccne2*
Foxo3	*Tef*	*Sgol1*	*Mcm4*
Ezh1	*Dicer1*	*Pcna*	*Rrm2*
Prdm5	*Bcas3*	*Top2a*	*Cycs*
Ptov1	*Ddx3y*	*Mtch2*	*Slc25a5*
Zfp30	*Gabarapl1*	*H2afz*	*Capza1*
Zbtb20	*Gltscr2*	*Hadhb*	*Idh3a*
Phf1	*Itm2a*	*Kpna2*	*Pgk1*
Il18	*Gstk1*		
Ddt	*Chkb*		
Ivd	*Pink1*		
Fhl1	*Ulk2*		
Ndrg2	*Dnajb9*		
Grina	*Pfdn5*		
Pik3r1	*Ctsf*		
Fyn	*Crim1*		
Ephx1	*Sepp1*		
Clstn1	*Gabbr1*		
Igf2r	*Rnf167*		
Selenbp1	*Map1lc3a*		

Supplementary Table 5. Quiescent stem cell gene signature as described in Cheung & Rando et al. in *Nat. Rev. Mol. Cell Biol (2013).*

Name	Sequence
EcoRI-[CA]30-XhoI Top	AATTCCACACACACACACACACACACACACACACACACACACACACACAC
EcoRI-[CA]30-XhoI BotRFP	TCGAGTGTGTGTGTGTGTGTGTGTGTGTGTGTGTGTGTGTGTGTGTGTGG
EcoRI-out of frame spacer-XhoI Top	AATTCCGATACCAGCTTAGATCGAAATTGC
EcoRI-out of frame spacer-XhoI BotRFP	TCGAGCAATTTCGATCTAAGCTGGTATCGG
EcoRI-[G]24-XhoI Top	AATTCGGGGGGGGGGGGGGGGGGGGGGC
EcoRI-[G]24-XhoI BotRFP	TCGAGCCCCCCCCCCCCCCCCCCCCCCG
EcoRI-[G]33-XhoI Top	AATTCGGGGGGGGGGGGGGGGGGGGGGGGGGGGC
EcoRI-[G]33-XhoI BotRFP	TCGAGCCCCCCCCCCCCCCCCCCCCCCCCCCCG

Supplementary Table 6. DNA sequences of oligonucleotides used to generate synthetic STRs.

Antibody	Clone	Company
anti-CD8α-PerCP/Cyanine5.5	53-6.7	Biolegend
anti-TCR Vb5.1 Vb5.2-PE/Cy7	MR9-4	Biolegend
anti-CD45.2-Alexa Fluor700	104	Biolegend
anti-CD27-Brilliant Violet 650	LG.3A10	Biolegend
anti-CD27-Brilliant Violet 421	LG.3A11	Biolegend
anti-CD27-APC	LG.3A11	Biolegend
anti-KLRG1-Brilliant Violet 421	2F1/KLRG1	Biolegend
anti-KLRG1-PE	2F1/KLRG1	Biolegend
anti-CD62L-Brilliant Violet 785	MEL-14	Biolegend
anti-CX3CR1-APC	SA011F11	Biolegend
anti-CD43-APC/Cy7	1B11	Biolegend
anti-IL2-Alexa Fluor 647	JES6-5H4	Biolegend
anti-IFNγ-Brilliant Violet 785	XMG1.2	Biolegend
anti-TNFα-Brilliant Violet 650	MP6-XT22	Biolegend
anti-CD107a- Alexa Fluor 647	1D4B	Biolegend
anti-CD107b- Alexa Fluor 647	M3/84	Biolegend
anti-Ki67-APC	B56	BD Biosciences
anti-CD19-biotin	6D5	Biolegend
anti-CD20-biotin	SA275A11	Biolegend
anti-CD4-biotin	GK1.5	Biolegend

Supplementary Table 7. Antibodies used in this study.

SUPPLEMENTARY NOTES

Supplementary Note 1| Division-coupled stochastic labeling as a proxy of division history

If we would consider a hypothetical T cell response comprising of two independent populations (A and B; see cartoon below): Both populations start dividing at time-point 1 with the same amount of RFP label. Population A undergoes a large amount of expansion, and subsequently stops dividing and contracts significantly. Population B undergoes a low level of proliferation, but experiences no contraction. At the time-point of measurement (time-point 3), population A and B have an equal size.

Due to the high level of proliferation in population A, it accumulates a larger amount of RFP$^+$ cells at time-point 2 as compared to its counterpart. As population A stops dividing, it stops accumulating RFP$^+$ cells. Next, because RFP labeling occurred stochastically, contraction will occur to the same extent in the labeled and the unlabeled cell pool. As a result, the two equally sized populations that are analyzed at time-point 3 will contain different fractions of RFP$^+$ cells, which reflect the difference in division history between these populations.

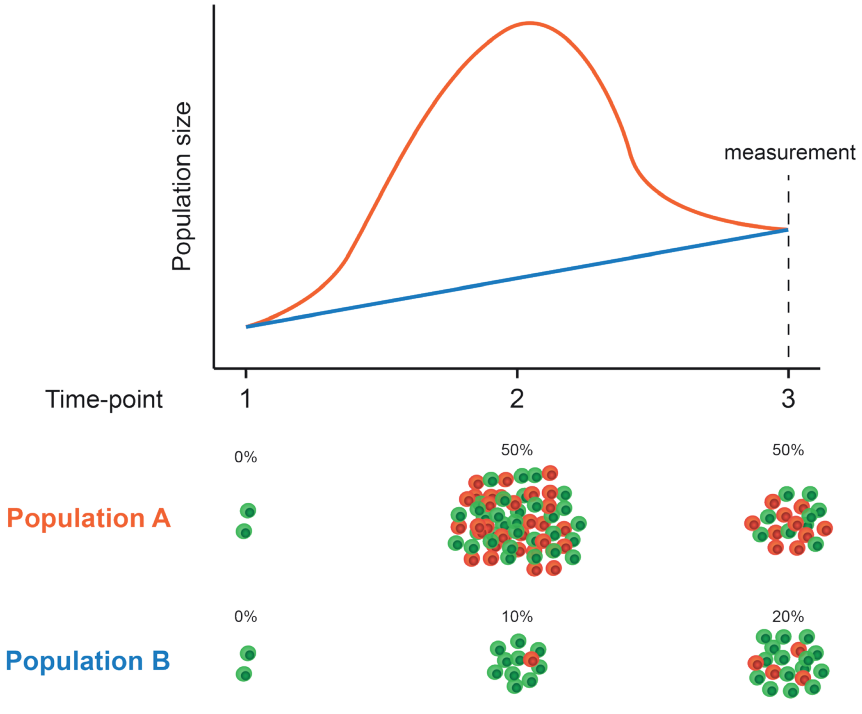

Supplementary Note 2

Minimal ODE model (Fig. 1b-d, i)

We detail the results from Weber et al[1], as originally shown for a branching process for a system of ordinary differential equations (ODEs). As in Weber et al[1], the average generation number is defined as the mean of the generation numbers of all the cells in the population.

For cells dividing at a rate λ/day and dying at a rate *d*/day, according to the ODE $\frac{dN}{dt} = (\lambda - d)N$, the equations for change in unlabeled (DR^{GFP}, *G*) and labeled (DR^{RFP}, *R*) cells with time can be written as

$$G' = (2-k)\lambda G + k\lambda(1-p)G - \lambda G - dG$$
$$R' = k\lambda pG + 2\lambda R - \lambda R - dR \quad (1)$$

the fraction of DR^{RFP} labeled cells, *fr* at time *t* is

$$f_R(t) = 1 - f_G(0)e^{-k\lambda pt} \quad (2)$$

where, *p* is the labelling probability and *k* is the number of daughter cells that get labeled. $k = 1$ is the asymmetric case when only one daughter cell can be labeled during cell division, and $k = 2$ is the symmetric case when both daughters can get labeled during cell division.

In such a model the average generation number, $\mu_t = 2\,\lambda t$, is independent of the death rate[2]. For this ODE, the relationship between the fraction of DR^{RFP} labeled cells in a population and its average generation number at some time-point *t* is

$$\mu_t = 2\lambda t = -\frac{2}{kp} ln\left(\frac{f_G(t)}{f_G(0)}\right) \quad (3)$$

MEF experiment described in Fig. 1h-i

Linear regression on the cell number data from the MEF experiment was used to infer the division rate λ (**Fig. I**). Using the same minimal ODE and assuming no cell death, the estimate for the division rate in the MEF data is λ = 0.698/day. The 95% confidence interval for the fit is 0.673-0.723.

With the division rate known, **Eq. (2)** was fitted to the fraction of DR^{RFP} labeled cells to estimate the switching probability *p*. **Fig. 1i** shows the fits of 300 bootstraps (100 per MEF experiment) on the MEF data. The basic statistics of the switching probability estimates from these fits are $p = 0.0053$ (mean), 0.0052 (median), 0.0043-0.0063 (95% CI).

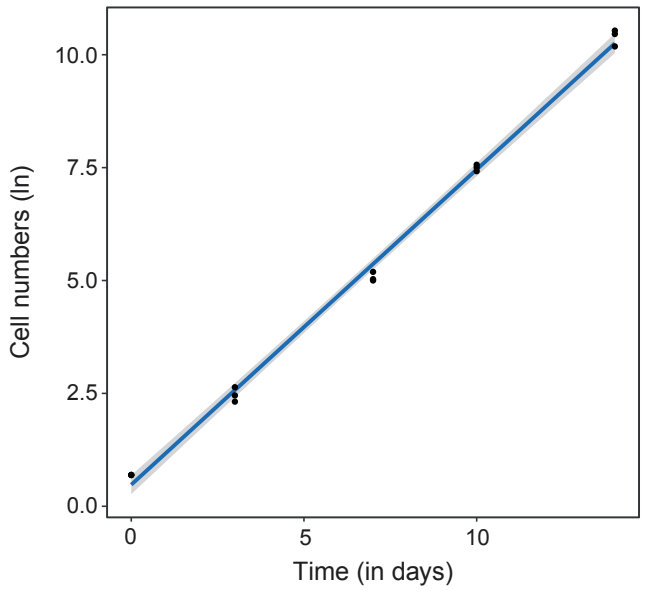

Figure I: Immortalized DivisionRecorder$^+$ (DR$^+$) mouse embryonic fibroblasts were cultured, counted, and analyzed every 3-4 days. Natural log of the number of DR$^+$ cells is shown for three experimental replicates. Black dots represent the experimental data, the best fit of the linear regression is depicted by the blue line, greyed area represents the 95% confidence interval. The slope of this regression line is the division rate of the cells in the MEF experiment.

Supplementary Note 3 | Expected DR^{RFP} fraction in the memory T cell pool (Extended Data Fig. 1)

In **Extended Data Fig. 1** we model the expected DR^{RFP} fractions in the memory T cell pool for a several scenarios where memory is generated from a subset of T cells that have undergone different a different number of divisions during the effector phase.

Consider the clonal expansion and subsequent contraction of a T cell population with two phenotypes: activated A cells and quiescent Q cells. Activated cells divide at a rate λ_A = 2/day for 6 days (expansion phase), die at a rate d_A = 0.2/day throughout, and can differentiate into quiescent cells at a rate a_i during the expansion phase. One daughter cell of a dividing unlabeled cell (DR^{GFP}, X_G) can become permanently labeled (DR^{RFP}, X_R) with a switching probability p = 0.0013. The labelling is genetic i.e., the daughters of a labeled cell cannot be unlabeled. In the model below, $i \geq 0$ denotes the division number.

$$
\begin{aligned}
A'_{G_{i+1}} &= \lambda_A A_{G_i} + (1-p)\lambda_A A_{G_i} - (\alpha_i + \lambda_A + d_A) A_{G_{i+1}} \\
A'_{R_{i+1}} &= p\lambda_A A_{G_i} + 2\lambda_A A_{R_i} - (\alpha_i + \lambda_A + d_A) A_{R_{i+1}} \\
Q'_{G_{i+1}} &= \alpha_i A_{G_{i+1}} \\
Q'_{R_{i+1}} &= \alpha_i A_{R_{i+1}}
\end{aligned}
\tag{4}
$$

We analyze two variants of the model. In the first variant, activated cells can only become quiescent when they have completed less than or equal to n divisions. In the second variant, we allow quiescent cells to be formed from activated cells throughout the expansion phase regardless of their prior division number (referred to as `all'). To create a similar number of quiescent cells in all cases we adjust the rate at which quiescent cells are formed. We depict two examples of the first variant in **Extended Data Fig. 1** (left and middle panels): n = 10 and n = 24 (i.e., in the left panel we set a_i = 0.25/day when $i < 10$ (and $t < 6$ days), and $a_i = 0$ otherwise, and in the middle panel we set a_i = 0.1/day when $i < 24$ (and $t < 6$ days), and $a_i = 0$ otherwise). The second variant shown in **Extended Data Fig. 1** (right panel) has the lowest rate at which quiescent cells are formed, a_i = 0.05/day for all i.

By numerical integration of **Eq. (4)**, we show in **Extended Data Fig. 1** that if the population that is persisting during the memory phase were composed of quiescent cells only, the percentage of DR^{RFP} labeled cells would decrease after the peak, regardless of when quiescent cells appear. Naturally, the decrease in the percentage of DR^{RFP} labeled cells after the peak is smaller when more quiescent cells are formed during the expansion phase. Note that we would not obtain much more quiescent cells if we would increase a_i in the n = 10 scenario because a too large a_i cripples the expansion of the activated cells.

Supplementary Note 4 |Reduction in DR^{RFP} fractions during recall responses (Fig. 6)

In **Figure 6** we apply the DivisionRecorder to assess the replicative recall potential of high- and low-division memory T cells, in situ. Based on the reduction in the fraction of DR^{RFP} cells that we reproducibly observe early upon recall, we conclude that secondary T_{EFF} cells predominantly derive from low-division T_{CM}, a conclusion that is in line with the data obtained using a CTV-based serial transfer approach (**Fig. 5**).

As a potential alternative explanation for the observed reduction in DR^{RFP} fractions, it could be proposed that recall responses would be based on the output of only a very small pool of memory T cells, and the numerical dominance of GFP-positive cells over RFP-positive cells (92.5% versus 7.5%, respectively) would make it likely that such cells would all be GFP-positive, even if replicative recall potential was identical for GFP-positive cells and RFP-positive cells. To determine how small the responding cell pool would have to be to achieve a reproducible drop in the fraction of DR^{RFP} cells without occasional 'jackpot events', in which one of the early responders would be RFP-positive (thereby resulting in a secondary T_{EFF} pool that is largely RFP-positive, something that is not experimentally observed), we modelled memory pools with 7.5% RFP-positive cells, responding to a secondary infection, allowing various numbers of these cells to expand, and then assessed the DR^{RFP} fractions within the resulting T_{EFF} pools (**Figure II**). This analysis indicates that secondary T_{EFF} pools generated from a very small precursor pool (< 20 cells) would show a reduction in DR^{RFP} fraction in the majority of mice, even if replicative recall potential would be equal between low-division and high-division T_{CM} populations. However, models that assume such a tight bottleneck do show the occurrence of jackpot events, an observation that is inconsistent with the experimental data (**Fig. 6**). In addition, an assumption of a responding cell pool of < 20 cells is inconsistent with the widely held view that recall responses are more rapid because of the larger pool of responding cells. Based on this analysis, we conclude that the observed drop in labeling rate during recall responses cannot be explained by T cell expansion during recall responses being driven by a very small pool of reactivated T cells.

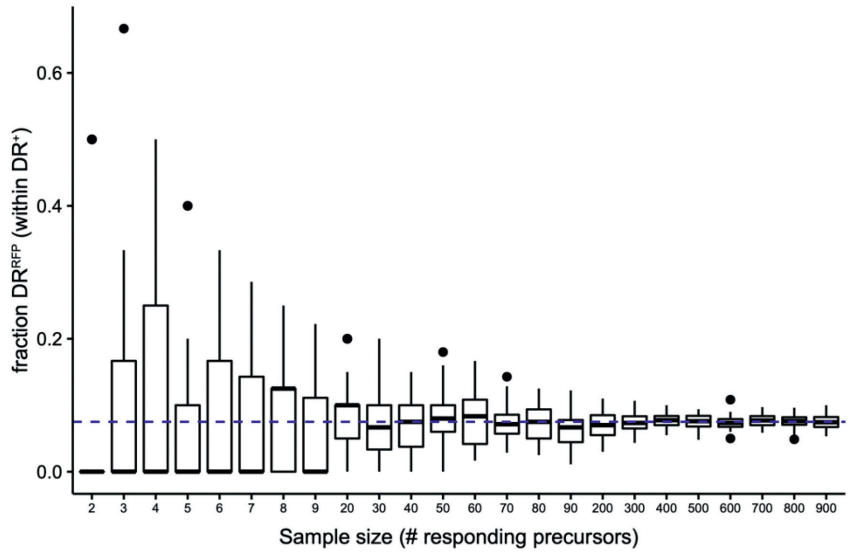

Figure II. Random sampling of precursor cells initiating the recall response. Expected DR^{RFP} fractions in secondary T_{EFF} pools (vertical axis) when a random sample of responding cells of a particular size (horizontal axis) is selected from a memory population that contains 7.5% DR^{RFP} cells (marked by horizontal dashed line). Selected responding cells expand to an equal degree to form the secondary T_{EFF} pool. Simulations were repeated 39 times (i.e., the number of mice in which recall experiments were performed in this manuscript). Boxplots indicate group median and 25th/75th percentiles, whiskers indicate the interquartile range multiplied by 1.5. Outliers are shown as dots.

Supplementary Note 5 | Phenotype model (Extended Data Fig. 2h, Fig. 7a-c, Extended Data Fig. 8)

In the main text, we argue that the observed drop in DR^{RFP} percentages is due to the preferential recruitment of lowly divided cells into subsequent responses. Here, we provide support for this proposition by demonstrating that a similar transient drop in DR^{RFP} frequencies is observed in mechanistic mathematical models that have a preferential recruitment of lowly divided cells into the secondary response. In the modeled T cell responses described below we consider two major phenotypic subsets; $CD27^{HI}$ $KLRG1^{LO}$ (hereafter referred to as T_{MULT}) and $CD27^{LO}$ $KLRG1^{HI}$ (hereafter referred to as T_{TERM}).

For an experiment in which DR^{RFP} label flow is asymmetrical and permanent, the DR^{RFP} accumulation in a population can be modelled by **Eq. (5)**; see the cartoon in **Extended Data Fig. 8a**. We model five phenotypes: clonally expanding activated T_{MULT}s (M_A), clonally expanding activated T_{TERM} s (E_A), cycling T_{MULT} s (M_C), cycling T_{TERM}s (E_C) and quiescent T_{MULT} s (M_Q, M_{nQ}). The variable M_{nQ} (for newQ) keeps track of newly formed quiescent cells to prevent them from becoming re-activated during the same expansion phase. These cells become M_Q during the contraction and memory phase and can be re-activated during the secondary expansion phase.

Upon encountering antigen, a naïve T cell becomes activated, starts dividing and gives rise to a continuum of phenotypically different populations. The phenotype model (**Extended Data Fig. 8a**) broadly classifies this continuum into the five phenotypes introduced above. An activated T_{MULT} can either differentiate into an activated T_{TERM} or can stop dividing and become a quiescent T_{MULT}. After the peak of the response, a small part of the activated T_{MULT}s and T_{TERM}s becomes cycling T_{MULT}s and long-lived T_{TERM}s, respectively. During the recall response, we model a scenario in which a fraction of the cells engages in renewed expansion. Upon secondary antigen encounter (set at day 86 post primary infection, in concordance with the recall experiment presented in **Fig. 6b**), the model undergoes a second sequence of expansion, contraction, and memory formation.

To examine the scenario in which lowly divided cells are preferentially recruited, it was important to know the division history of cells prior to the re-expansion. We, therefore, formulated a division-indexed model (similar to **Eq. 4**) to track the number of divisions of the DR^{GFP} and DR^{RFP} cells of each phenotype over time. The model is described in full in the supplementary R codes. For readability we here present a collapsed version of the model, which can be obtained by summing over the division numbers as well as the DR^{GFP} and DR^{RFP} cells (compare the full model equations shown in **Eq. (6)** to the collapsed equation in **Eq. (5)** for a single phenotype, E_A):

$$\frac{dM_A}{dt} = \alpha(i)r\left(M_C + M_Q\right) + 2\lambda_A M_A - \left(\lambda_A + d_A + \delta_E(t) + \delta_Q(t) + \mu_C\right)M_A$$

$$\frac{dE_A}{dt} = \delta_E(t)M_A + 2\lambda_A E_A - (\lambda_A + d_A + \mu_C)E_A$$

$$\frac{dM_C}{dt} = \mu_C M_A + 2\lambda_M M_C - (\lambda_M + d_M + \alpha(i)r + (1-\alpha(i))d_C)M_C$$

$$\frac{dE_C}{dt} = \mu_C E_A + 2\lambda_E E_C - (\lambda_E + d_E + d_C)E_C$$

$$\frac{dM_{nQ}}{dt} = \delta_Q(t)M_A - \mu_Q M_{nQ} \quad (5)$$

$$\frac{dM_Q}{dt} = \mu_Q M_{nQ} - (\alpha(i)r + (1-\alpha(i))d_C)M_Q$$

$$\delta_E(t) = \delta_{E_{max}}(1 - e^{-e_a t_{exp}})$$

$$\delta_Q(t) = \delta_{Q_{max}} e^{-m_q t_{exp}}$$

$$\alpha_i = \left(1 + \left(\frac{i}{h}\right)^m\right)^{-1};\ i = 1, \ldots, n$$

where t_{exp} (for time in expansion) is the time since the most recent challenge. The fraction of cells that is expected to be re-activated, $0 \le a(i) \le 1$, is a function of the division number, i. Each phenotype is actually indexed by the number of divisions completed, i, and is subdivided into an unlabeled (DR^{GFP}, R) and a labeled (DR^{RFP}, G) subtype. For instance, the full division-indexed model for activated T_{TERM}s is:

$$\frac{dE_{A_{G_i}}}{dt} = \delta_E(t)M_{A_{G_i}} + (2-p)\lambda_A E_{A_{G_{i-1}}} - (\lambda_A + d_A + \mu_C)E_{A_{G_i}} \quad (6)$$

$$\frac{dE_{A_{R_i}}}{dt} = \delta_E(t)M_{A_{R_i}} + p\lambda_A E_{A_{G_{i-1}}} + 2\lambda_A E_{A_{R_{i-1}}} - (\lambda_A + d_A + \mu_C)E_{A_{R_i}}$$

where p is the switching probability. A complete list of division-indexed phenotype specified equations can be found in the R code. Below, we explain the step-wise parameter estimation procedure of this model.

Fitting the model and estimating the parameters

Two phases of immune response were inferred from the experimental data: the expansion phase (day 0-6 for the primary response and day 86-90 for the secondary response), and the non-expansion phase, i.e., the contraction and memory phases (day 6-86 for the primary response and day 90-111 for the secondary response). The percentages of DR^{RFP} cells in blood and spleen were found to be highly similar. Additionally, the ratio of the number of DR^{GFP} cells in spleen to that in blood was similar across all time points. The blood and spleen data were therefore fitted simultaneously under the assumption that both compartments are well-mixed (**Fig. 7a-c, Extended Data Fig. 8**).

Our primary interest was to find a realistic division history of all phenotypes on day 86, to subsequently test whether the preferential recruitment of lowly divided cells can explain the kinetics of labeling rate during recall responses. The number of free model parameters was reduced to 6 using a few simplifying assumptions:

(i) The division rate during the expansion phase is the same for T_{MULT}s and T_{TERM}s,

(ii) The death rate of cells during the expansion phase is negligible,

(iii) The formation of quiescent cells decreases with time post antigen encounter,

(iv) The rate at which T_{TERM}s are formed increases with time (instead of division number),

(v) Only 5% of the activated cells survive after the expansion phase, i.e., $\mu_C = \frac{d_A}{19}$, and

(vi) T_{MULT}s and T_{TERM}s maintain constant numbers during the memory phase, i.e., $\lambda_M = d_M$ and $\lambda_E = d_E$.

The free parameters were estimated by fitting the collapsed model sequentially to the data obtained during the primary expansion and non-expansion phases. First, the initial number of cells that were activated among the engrafted cells in blood and spleen, the division rate of the activated cells, and the differentiation rate of the activated cells into the different phenotypes were estimated using the experimental data obtained during the expansion phase. Next, these estimated parameters were used to estimate the division rates of the cycling cells from the experimental data obtained during the non-expansion phase. Because the estimation of the re-activation function was infeasible, as it would require fitting the full division-indexed model to the data, this function was tuned manually to obtain an optimal description of the data with the full model. The estimated parameters for the best description of the data are listed in Table S1.

Expansion of adoptively transferred DR^+ cells is expected to occur after a short delay, covering both the time required to identify an antigen-positive APC and to initiate cell division after TCR triggering. This delay was fixed to 1 day as our dataset lacked the appropriate information for this parameter to be estimated. The loss rate of activated cells was fixed to $d_A = 0.3$/day. The rate at which the formation of quiescent cells declines was tuned such that only 1% of the quiescent population formed during the primary response would be DR^{RFP}. As antigen-experience is known to influence secondary memory formation, e.g. the expansion phase occurring on a shorter time-scale and a considerably slower contraction phase, the rates during the secondary response differ from those during the primary response[3]. Therefore, m_q and μ_c were set to 0.5/day and $\frac{d_A}{4}$, respectively.

The maximum rate at which quiescent cells were formed was fixed to different values ($\delta_{Q_{max}} \in \{0.01,\ 0.1\}$) to generate different numbers of quiescent cells (10^3, 10^4) at the peak of the primary response (day 6) (**Fig. 7a**). Unsurprisingly, formation of a larger number of quiescent cells during the primary response, resulted in a larger drop in DR^{RFP} frequencies during secondary expansion (**Fig. 7b**). Higher numbers of quiescent T_{CM} also generated secondary responses that were higher in magnitude, providing a better explanation of the data (**Extended Data Fig. 8b-d**). Three different re-activation functions, signifying either an abrupt (fun 1-2) or gradual loss (fun 3) of re-expansion potential based on the number of prior divisions, were tested (**Fig. 7a**). The experimental data was only congruent with scenarios where re-expansion potential was restricted to cells that had undergone limited clonal expansion (**Fig. 7a-b**). Furthermore, higher numbers of quiescent T_{CM} correlated positively with larger drops in DR^{RFP} frequencies upon re-expansion (**Fig. 7b**).

Parameter	Description	Value	Units	On (1)/Off (0) during phases	
				Expansion	Non-expansion
t_{on}	Time delay before the first division	1 (F)	days	-	-
λ_A	Division rate of activated T_{MULT} and T_{TERM} cells	0.89	/day	1	0
d_A	The rate at which (re-) activated T_{MULT} and T_{TERM} cells leave circulation	0.3 (F)	/day	0	1
d_C				1	0
δ_{Qmax}	Maximum differentiation rate of the activated T_{MULT} into quiescent T_{MULT} cells	0.1 (F)	/day	1	0
m_q	The rate at which $\delta_Q(t)$ changes	0.25 (F)	/day	-	-
δ_{Emax}	Maximum differentiation rate of the activated T_{MULT} into activated T_{TERM} cells	2 (F)	/day	1	0
e_a	The rate at which $\delta_E(t)$ changes	0.15	/day	-	-
$\lambda_M = d_M$	Division and death rate of the cycling T_{MULT} cells	0.3	/day	1	1
$\lambda_E = d_E$	Division and death rate of the cycling T_{TERM} cells	0.04	/day	1	1
r	The rate of re-activation of quiescent and cycling T_{MULT}s	1 (F)	/day	1	0
h	Cut-off of the fraction re-activated function	25 (F)	-	-	-
m	Slope of the fraction re-activated function	30 (F)	-	-	-
$M_{A_G}(0)$	Initial number of naïve cells at day 0	16748.72 (Spleen)	Cells (avg.)	-	-
		149.30 (Blood)			

Table S1: The estimated parameters for the best fit of the phenotype model to the data. The parameter values in this table were obtained by fitting the phenotype model to the blood and spleen data simultaneously using the pseudorandom-search algorithm (see pseudoOptim) in the modFit function of the FME R package[4]. F signifies that these parameters were set to a fixed value.

Supplementary Note 6 | Analysis of DivisionRecorder single integration frequency

As the DivisionRecorder is retrovirally introduced into the genome, a fraction of the modified cells may carry multiple integrations. As each DivisionRecorder has an independent probability of slippage—and hence creation of an in-frame *Cre* gene—during cell division, this means that cells that contain more than 1 integration will have a 'faster clock', resulting in the more rapid labeling of these cells. However, as the DivisionRecorder is applied as a population-based metric, and conclusions are based on comparison of different timepoints and/or different cell populations within individual mice, the presence of a fraction of cells with multiple integration events will not influence the interpretation of the obtained data. Nevertheless, to minimize variation in the fraction of cells with >1 integration event between experiments, we aimed for a low and standardized transduction efficiency, in which the occurrence of multiple integration events will be minor. To determine which fraction of single integrations could be expected as a factor of transduction efficiency, Ai9 mouse embryonic fibroblasts (MEFs) or ex vivo activated Ai9;OT-I cells were transduced with a mixture of 2 retroviruses encoding either GFP or Katushka. The fraction of single and double-positive cells could subsequently be used to estimate the relationship between transduction efficiency and the percentage of single integrations. This analysis shows that at a transduction efficiency of ~10-15% (the transduction efficiency used for in vivo experiments), approximately 85-90% of the modified cells contains a single integration, and this percentage is comparable between the two cell types assessed (**Figure III**). Thus, the large majority of switch events we observe in our experiments derives from cells carrying a single reporter.

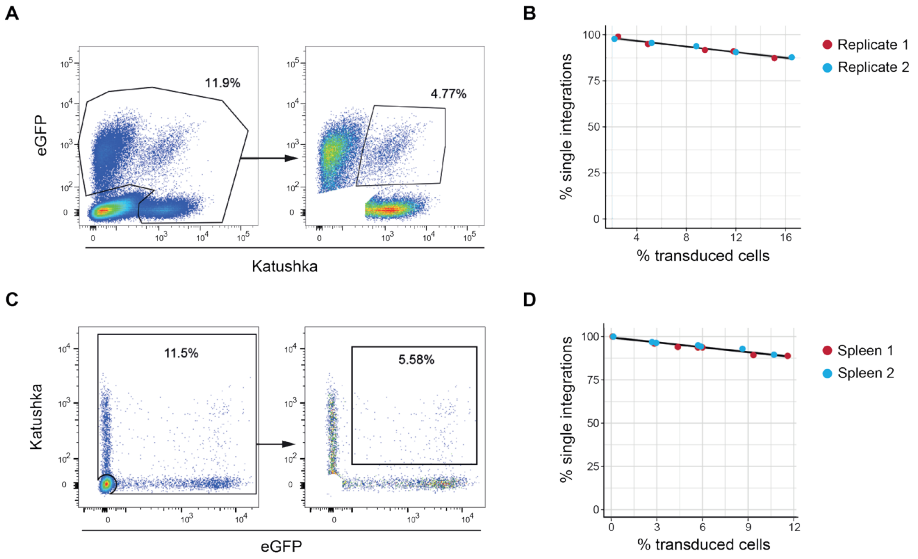

Figure III. Frequency of multiple retroviral integration events. GFP and Katushka encoding retroviruses were mixed 1:1, and subsequently used to transduce either Ai9 MEF cells (**A-B**) or ex vivo activated Ai9;OT-I cells (**C-D**). Ai9 MEF and Ai9;OT-I cells were assessed for fluorescent protein expression at day 7 or 24 hours post transduction, respectively. The percentage of cells carrying a single integration was calculated as 100-(2*fraction GFP$^+$Katushka$^+$ cells). **A**) Gating strategy to determine the percentage of GFP$^+$Katushka$^+$ cells within the transduced Ai9 MEF cell population. **B**) Plot depicting the percentage of Ai9 MEF cells carrying a single retroviral integration at different transduction efficiencies. **C**) Gating strategy to determine the percentage of GFP$^+$Katushka$^+$ cells within the transduced Ai9;OT-I cell population. **D**) Plot depicting the percentage of Ai9;OT-I cells carrying a single retroviral integration at different transduction efficiencies. Depicted data was obtained in a single experiment consisting of two experimental replicated. Dots indicate individual samples, lines represent a linear regression fitted to the data points (**B, D**).**Supplementary Note 7 | Retroviral silencing of the DivisionRecorder does not occur**

As the GFP-Cre module of the DivisionRecorder is introduced retrovirally, there is a potential risk of retroviral transcriptional silencing or attenuation. Such silencing events could influence interpretation of the data, as the fraction of DR^{RFP} cells over DR^{GFP} cells may become skewed. As only the GFP-Cre module is retrovirally introduced, whereas the RFP reporter that is switched on upon Cre activity is germline encoded, the extent of retroviral silencing can be experimentally determined by measuring the occurrence of cells that do show RFP expression (and hence did at some point express the GFP-Cre module) but lack GFP expression. As depicted in **Figure IV**, virtually no RFP$^+$GFP$^-$ cells are observed within recipient mice, either during the acute phase or in the memory phase, demonstrating that retroviral silencing is extremely rare.

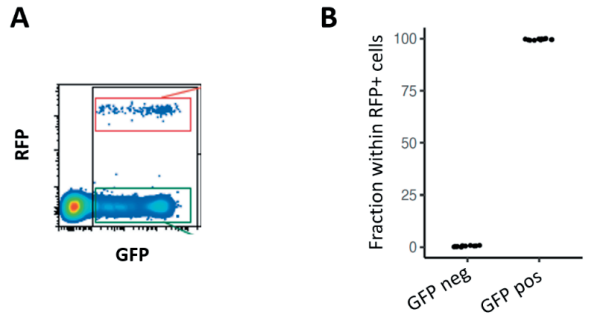

Figure IV. GFP expression of RFP$^+$ cells. LM-OVA infected recipient mice received 20,000 DR$^+$ cells and the occurrence of GFP$^-$RFP$^+$ cells was assessed in spleen on day 6 and 86 after adoptive cell transfer. **A**) Flow cytometry plot, gated on CD45.2$^+$ cells, depicting RFP and GFP expression. **B**) Fraction of GFP$^-$ and GFP$^+$ cells within the RFP$^+$ cell population (n=12 mice).

REFERENCES SUPPLEMENTARY NOTES

1. Weber, T. S., Perié, L. & Duffy, K. R. Inferring average generation via division-linked labeling. *J Math Biol* **73**, 491–523 (2016).
2. De Boer, R. J. & Perelson, A. S. Quantifying T lymphocyte turnover. *J. Theor. Biol.* **327**, 45–87 (2013).
3. Masopust, D., Ha, S.-J., Vezys, V. & Ahmed, R. Stimulation History Dictates Memory CD8 T Cell Phenotype: Implications for Prime-Boost Vaccination. *J Immunol* **177**, 831–839 (2006).
4. Soetaert, K. & Petzoldt, T. Inverse Modelling, Sensitivity and Monte Carlo Analysis in *R* Using Package **FME**. *J. Stat. Soft.* **33**, (2010).